Scattering of He^3 by He^4 and of He^4 by Tritium*

R. J. SPIGER AND T. A. TOMBRELLO
California Institute of Technology, Pasadena, California
(Received 29 May 1967)

The differential elastic scattering cross section has been measured for the scattering of He^3 from He^4 and the scattering of He^4 from tritium for bombarding energies of 5 to 18 and 4 to 18 MeV, respectively. Data were also obtained for the reactions $He^4(He^3,p)Li^6$, $He^4(He^3,p')Li^{6*}$, $H^3(\alpha,n)Li^6$, and $H^3(\alpha,n')Li^{6*}$. Levels are seen at 4.65, 6.64, 7.47, and 9.7 MeV in Li^7, and at 4.57, 6.73, 7.21, and 9.3 MeV in Be^7. A phase-shift analysis suggests assignments of $\frac{7}{2}^-$ and $\frac{5}{2}^-$ for the two lower levels in Li^7, confirms the $\frac{5}{2}^-$ assignment of the 7.47 level, and suggests a $\frac{7}{2}^-$ assignment for the new level at 9.7 MeV. Similarly in Be^7, the assignments of $\frac{7}{2}^-$ and $\frac{5}{2}^-$ for the lower two levels are confirmed, and an assignment of $\frac{7}{2}^-$ is suggested for the new level at 9.3 MeV. The reduced widths for α and nucleon emission were determined by fitting the phase shifts near each level with a single- and/or double-level formula from the R-matrix formalism of Lane and Thomas. The results of the analysis are discussed and compared with predictions of recent nuclear-model calculations.

I. INTRODUCTION

In the past few years, several experimental studies of the excited states of the compound nuclei Li^7 and Be^7 have been made. The work to be described was designed to complement and extend the range of these studies. The ONR-CIT tandem accelerator was used to produce He^4 and He^3 beams at energies up to 18 MeV, allowing the compound nuclei to be investigated over a wide energy range.

The entrance channels employed in this investigation were $t+\alpha$ for Li^7 and He^3+He^4 for Be^7. From an experimental point of view these entrance channels have the advantage of allowing the use of gas targets, for which the data obtained could easily be given an absolute normalization. The theoretical analysis was also simplified by the fact that both entrance channels were cases of the scattering of a spin-$\frac{1}{2}$ particle from a spin-zero particle.

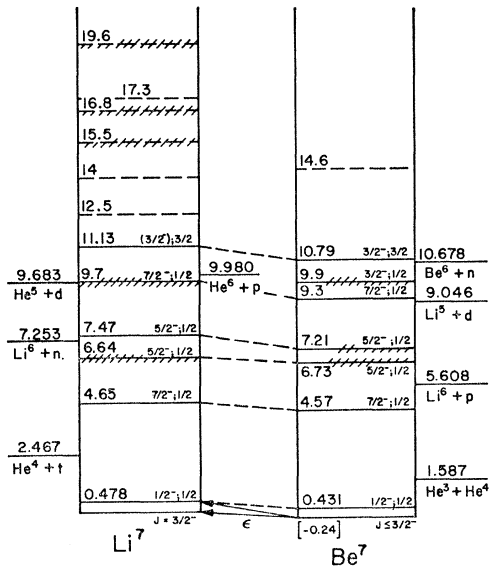

FIG. 1. Isobar diagram showing the energy levels of Li^7 and Be^7. The spins, parities, and isospins of the levels are also shown.

The entrance channels used lead to several reactions. (See Fig. 1.) For Li^7, the reactions $H^3(\alpha,\alpha)H^3$, $H^3(\alpha,n)Li^6$, and $H^3(\alpha,n')Li^{6*}$ were investigated. For Be^7, the analogous reactions $He^4(He^3,He^3)He^4$, $He^4(He^3,p)Li^6$, and $He^4(He^3,p')Li^{6*}$ were studied. An analysis of the data obtained made it possible to compare α widths and nucleon widths of several levels with predictions of the intermediate-coupling model.[1]

II. EXPERIMENTS

A. T(α,α)T

The tritium-gas target, for the $t-\alpha$ scattering, was contained in a small gas cell, 4.45 cm in diameter and 1.9 cm in height. Thin nickel foils were used as windows for the cell; the beam entrance foil was 8100-Åthick and the exit foils were ~13 000-Å thick. The cell was supported in the center of the scattering chamber by a tube, through which the tritium gas entered the cell or was pumped from it. The gas was normally stored in a reservoir in the form of uranium tritide; heating the uranium tritide was used to evolve tritium into the gas cell and the cool uranium acted as a pump to extract the tritium from the gas cell at the end of a run. A target gas pressure of 40-mm Hg was normally used.

The scattering chamber (Fig. 2) was constructed of a cylindrical steel pipe with top and bottom of aluminum. The walls were 1.9-cm thick and the inner diameter of the chamber was 27.9 cm. The chamber was provided with four ports set at 90° intervals around the chamber walls.

The beam enters through a collimator formed by a series of tantalum discs pierced with holes 1.5 or 2.0 mm in diameter. These serve to collimate the beam and provide resistance to the passage of gas from the chamber in the event of a leak in the gas cell. The opposite port leads to an electrostatically and magnetically suppressed Faraday cup used to collect the beam after passage

* Supported in part by the Office of Naval Research [Nonr-220(47)].

[1] F. C. Barker, Nucl. Phys. 83, 418 (1966).

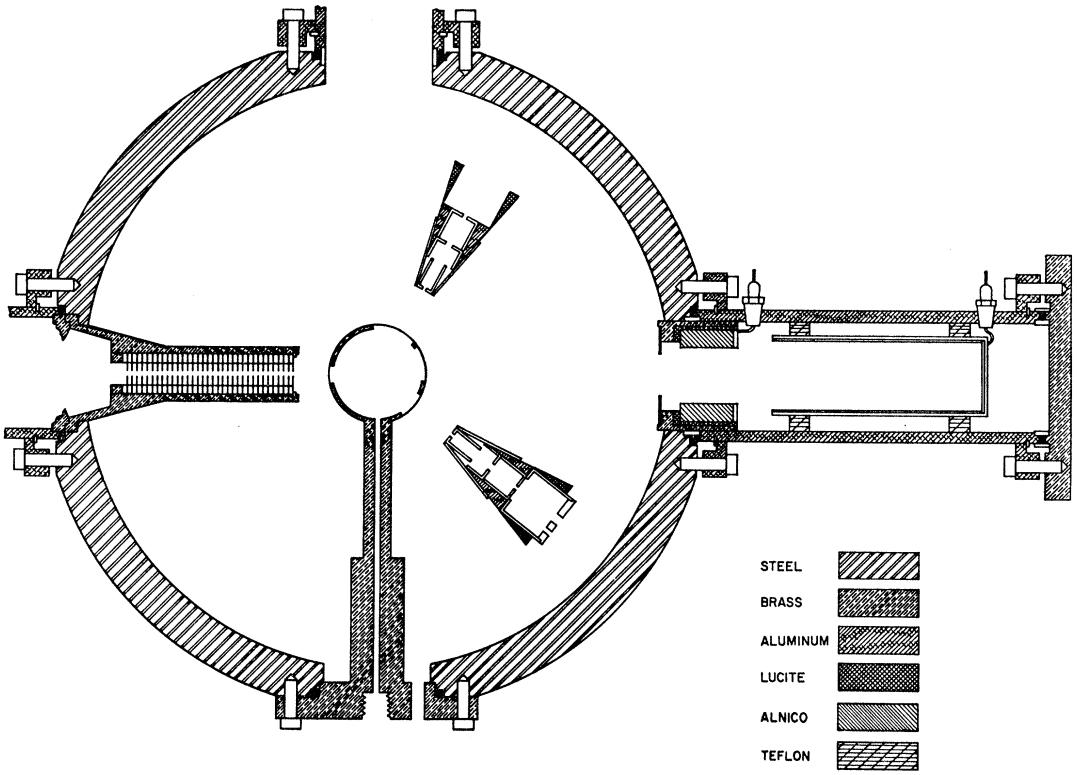

FIG. 2. The tritium chamber shown as seen from the top on a horizontal plane through the beam line.

through the target. The port opposite that containing the gas cell assembly leads to the main pumping station. It is also fitted with an ionization gauge which is used to monitor chamber pressure during the course of a run. The connection to the pumping station is closed when tritium is in the gas cell; with the valve closed, the chamber is held at a pressure of $\sim 5\times 10^{-6}$ Torr by a liquid-nitrogen-cooled activated charcoal trap.

Upstream from the beam collimator is another liquid-nitrogen-cooled charcoal trap followed by a second group of tantalum discs, which further increases the resistance to gas flow from the chamber. Beyond this second set of disks is an electrically operated safety valve which can isolate the chamber in case of a gas leak.

The top of the chamber is fitted with two movable counter arms, on which the detectors and their collimators were mounted. A thin (26–50 μ) surface-barrier detector was used in conjunction with a thicker surface-barrier detector to form a dE/dx, E telescope for the separation of hydrogen isotopes from helium isotopes.

Beam energies from 4 to 13.1 MeV were obtained from the ONR-CIT tandem accelerator by injecting neutral helium ions. Typical beam currents on target, after magnetic analysis and focusing were 200 nA. For beam energies of 13 to 18 MeV, negative helium ions were injected; typical beam currents on target were 15 nA. [In the $He^4(He^3,He^3)He^4$ experiment, it was possible to use the neutral injection beam up to 14.75 MeV.]

B. $T(\alpha,n)Li^6$ and $T(\alpha,n')Li^{6*}$

These reactions were investigated using a solid target of zirconium tritide on a platinum backing. A yield curve, proportional to the total cross section for the $T(\alpha,n)Li^6$ reaction, was obtained by placing a "long counter" very close to the target at 0°. The geometry was such that the counter intercepted all of the cone of neutrons over the energy range investigated, $E_\alpha = 11.0$ to 12.4 MeV. Angular distributions of the neutrons from $T(\alpha,n)Li^6$ were obtained using a stilbene crystal and a γ-ray discriminator circuit.[2]

A yield curve proportional to the total combined cross section for $T(\alpha,n)Li^6$ and $T(\alpha,n')Li^{6*}$ was obtained using a paraffin cylinder, 30 cm in diameter, as a moderator in conjunction with an NE 402 phosphor mounted on a phototube. The detector was on the axis of the cylinder which was set at 0° with respect to the target. In all three experimental arrangements, the target chamber was insulated to provide beam integration.

C. $He^4(He^3,He^3)He^4$

The chamber used in this experiment was quite similar to the chamber used in the $T(\alpha,\alpha)T$ experiment and has been described previously.[3] The beam integra-

[2] C. N. Davids, Ph.D. thesis, California Institute of Technology, 1967 (unpublished).
[3] T. A. Tombrello and L. S. Senhouse, Phys. Rev. 129, 2252 (1963).

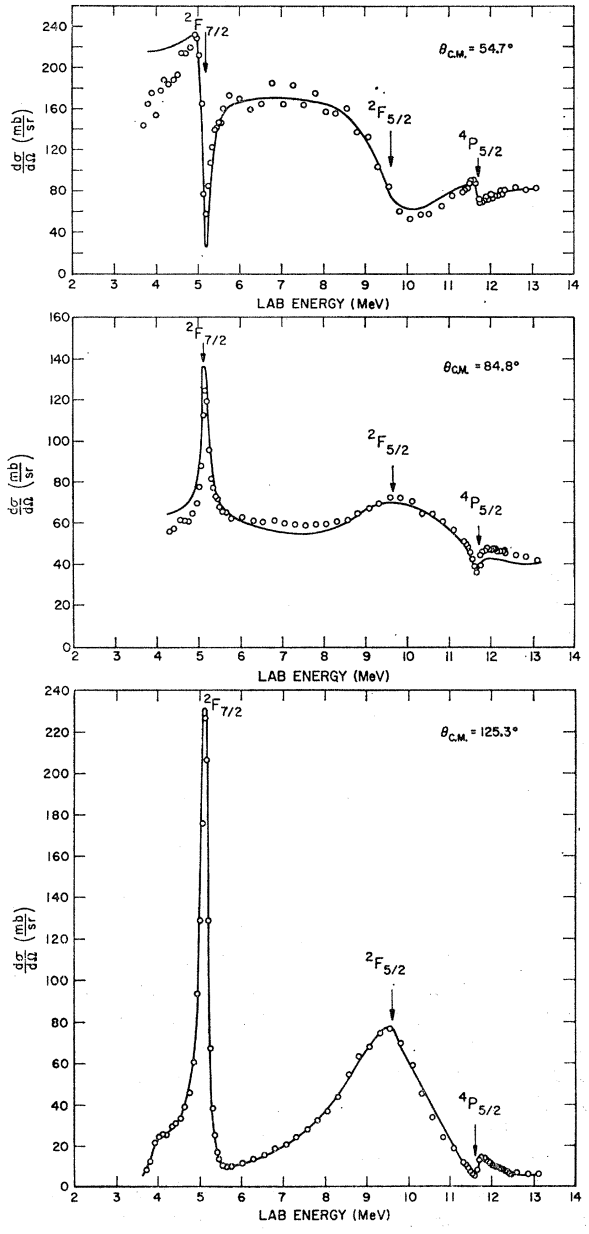

FIG. 3. Three typical excitation curves from the $H^3(\alpha,\alpha)H^3$ experiment below 13.2 MeV. The open circles show the experimental points and the solid line is a fit to the points from the phase shift analysis. The arrows indicate positions of levels in Li^7.

tion and particle detection were also basically the same as that used in the $T(\alpha,\alpha)T$ experiment.

For bombarding energies between 4.6 and 14.75 MeV, the chamber was completely filled with the He^4 target gas at a pressure of approximately 1-cm Hg. This low pressure was sufficient when the higher current of the neutral injection beam of the accelerator was used. For bombarding energies above 14.75 MeV, the low-current negative injection beam of the accelerator was used, requiring a higher pressure for the target gas. This was made possible by removing the 1000-Å Ni entrance foil and containing the target gas in a small gas cell at the center of the chamber. The beam entrance and exit windows of the cell were covered by thin nickel foils (6250 Å) and the scattered particles emerged through a 4-μ Mylar window. A pressure of 15-cm Hg was maintained in the cell.

D. $He^4(He^3,p)Li^6$ and $He^4(He^3,p')Li^{6*}$

The apparatus for these experiments was the same as that used for the $He^4(He^3,He^3)He^4$ experiment. Above 13.2-MeV bombarding energy, the gas-cell configuration was used. Below 13.2 MeV, the entire chamber was filled with gas at a pressure of approximately 2.3-cm Hg.

III. RESULTS

A. $T(\alpha,\alpha,)T$

Excitation curves of the differential elastic scattering cross section were obtained at 17 center-of-mass angles in the energy range from 3.6 to 13.1 MeV. Excitation curves at eight center-of-mass angles were obtained in the energy range from 12.8 to 18.2 MeV. Figure 3 shows three of the excitation curves obtained below 13.1 MeV. Data points are shown by the open circles. Data were taken at intervals of 50 keV over the narrow resonances and at 250-keV intervals elsewhere. These curves show clearly the narrow level at 5.2-MeV bombarding energy (4.65-MeV excitation energy in Li^7) and the broad level near 9.8 MeV (6.64 MeV in Li^7). The effect of the 7.47-MeV level in Li^7 appears as the small structure near 11-MeV bombarding energy.

Figure 4 shows three typical angular distributions generated from the excitation curves. These distributions were obtained below, at, and above the broad 6.64-MeV level in Li^7.

Figure 5 shows three typical excitation curves obtained above 12.8-MeV bombarding energy. A resonance is seen near 16.8-MeV bombarding energy corresponding to an excitation of 9.7 MeV in Li^7. Data were taken at 100-keV intervals from 16- to 18-MeV bombarding energy and at 250-keV intervals elsewhere. The solid lines in Figs. 3–5 indicate the results of the phase-shift analysis, which will be discussed in Sec. IV.

The experimental errors associated with these data are of two types. Systematic errors are primarily those associated with the apparatus, such as target density, integrator accuracy, and angular position accuracy. The relative errors are primarily due to the problems involved in background subtraction and statistics in the spectra. For the $T(\alpha,\alpha)T$ experiment, the major systematic error was due to the presence of hydrogen-gas contamination in the tritium target. The over-all systematic error was 3.2%. Relative errors resulted from difficulties in making a consistent background subtraction and from poor statistics at some of the minima in the excitation curves. Typical relative errors for the three curves of Fig. 3 (data for $E_\alpha \leq 13.1$ MeV) were

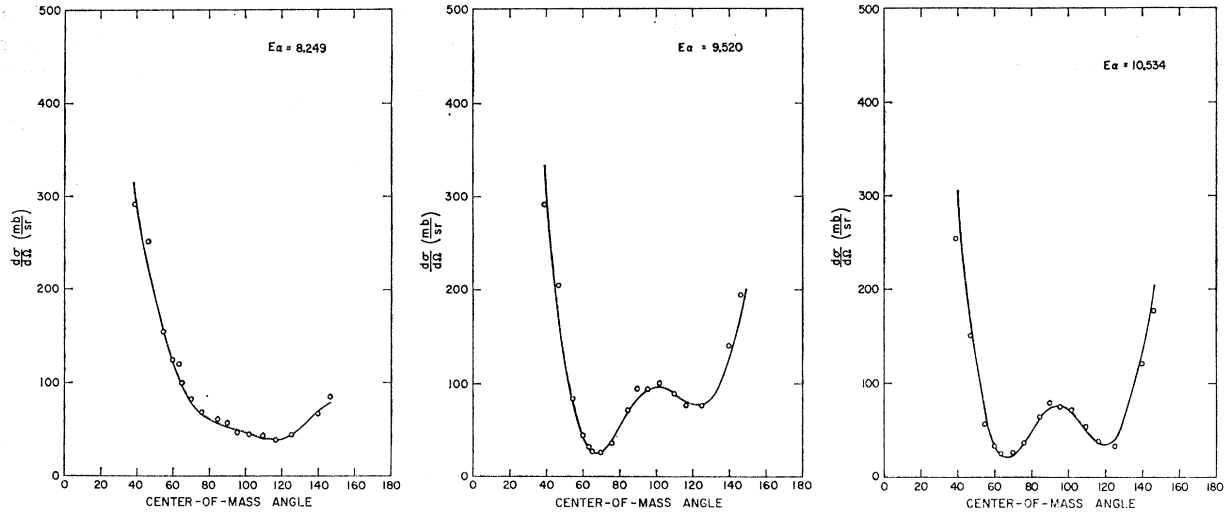

FIG. 4. Three typical angular distributions from the $H^3(\alpha,\alpha)H^3$ experiment. Symbols are the same as in Fig. 3.

8% (54.7°), 4% (84.8°), and 2% (125.3°). For the curves of Fig. 5 (data for $E_\alpha \geq 12.8$ MeV) typical relative errors were: 2% (54.7°), 2% (91.4°), and 3% (126.5°). The greatest relative errors generally occurred at the lowest beam energies, where the scattering from the gas cell and foils was significant.

B. $T(\alpha,n)Li^6$ and $T(\alpha,n')Li^{6*}$

A yield curve for the $T(\alpha,n)Li^6$ reaction was obtained from 11.0- to 12.4-MeV bombarding energy. The dominant effect is due to the resonance at 7.47 MeV in Li^7.

The combined total cross section for the reactions $T(\alpha,n)Li^6$ and $T(\alpha,n')Li^{6*}$ is shown in Fig. 6 as a function of bombarding energy. These data show the effect of the narrow 7.47-MeV level in Li^7 ($E_\alpha = 11.7$ MeV) and indicate a broader resonance near $E_\alpha = 16.8$ MeV. Below 16 MeV, the only open neutron channel is $T(\alpha,n)Li^6$. The data below this energy were normalized to the data of Schwarz *et al.*[4] on the inverse reaction $Li^6(n,\alpha)T$. The normalization of this region of data allowed us to normalize the higher-energy data above 16 MeV. A smooth background under the broad resonance was attributed to the $T(\alpha,n)Li^6$ reaction and subtracted. The remainder was assumed due to the $T(\alpha,n')Li^{6*}$ reaction. The total reaction cross section above 16.0 MeV has an accuracy of approximately ±30%.

Several neutron angular distributions and excitation curves for the reaction $T(\alpha,n)Li^6$ were obtained from 14.0 to 18.3-MeV bombarding energy. These data show no pronounced resonance behavior and their effect on the analysis of the data will be discussed in Sec. V.

C. $He^4(He^3,He^3)He^4$

Excitation curves of the differential elastic-scattering cross section were obtained at 14 center-of-mass angles between bombarding energies of 4.6 and 14.75 MeV. From 14.75- to 18.0-MeV, data were obtained at ten center-of-mass angles. Figure 7 shows three of the excitation curves obtained. The data points were taken at 50-keV intervals over the narrow resonance and at 250-keV intervals elsewhere. The narrow resonance near 5.2 MeV (4.57-MeV excitation energy in Be^7) and the broad resonance near 9 MeV (6.73 MeV in Be^7) are clearly seen. The 7.18-MeV level in Be^7 is not seen in the elastic scattering. A resonance is also seen near 13.5 MeV (9.3 MeV in Be^7).

Figure 8 shows three of the angular distributions generated from the excitation curves. These curves show angular distributions below, at, and above the broad resonance near 9-MeV bombarding energy. In both the excitation curves and the angular distributions, the solid curves show fits to the data from the phase-shift analysis.

The systematic errors for the curves in Fig. 7 were from 1.1 to 1.5%. Typical relative errors were: 2% (54.7°), 3% (90.0°), and 3% (125.2°).

D. $He^4(He^3,p)Li^6$ and $He^4(He^3,p')Li^{6*}$

The differential reaction cross section for the reaction $He^4(He^3,p)Li^6$ was obtained at bombarding energies from 8 to 18 MeV. Data were taken at intervals from 100 to 500 keV. Laboratory angles from 15° to 90° were investigated in steps of 5°. Other angles, corresponding to those for which elastic-scattering data were taken, were also investigated.

Figure 9 shows two excitation curves of the protons leaving Li^6 in its ground state. The resonance near 9.5 MeV shows the effect of the 7.18-MeV level in Be^7. An effect of the level at 9.3 MeV in Be^7 is seen in the 45° curve near 13.5 MeV. This effect was a maximum in the 45° curve. For the 22.5° curve, the systematic error was 1.5% and the relative errors were 2–4%. For the 45°

[4] S. Schwarz, L. G. Strömberg, and A. Bergström, Nucl. Phys. 63, 593 (1965).

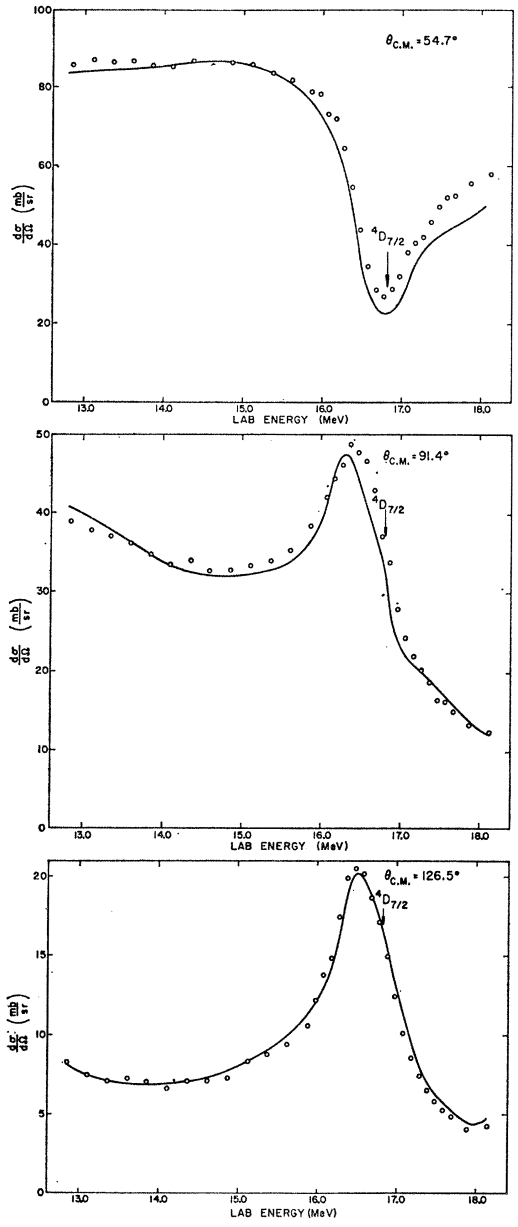

FIG. 5. Three typical excitation curves from the $H^3(\alpha,\alpha)H^3$ experiment above 12.8 MeV. Symbols are the same as in Fig. 3.

curve, the systematic error was 1.1% and the relative errors were 5–10%.

Similarly, the differential reaction cross section for the reaction $He^4(He^3,p')Li^{6*}$ was obtained from threshold near 11- to 18-MeV bombarding energy. Figure 10 shows excitation curves for two of the angles investigated. For both curves, the systematic error was 1.1%. The relative errors were 15%. The effect of the 9.3-MeV level in Be^7 is seen near $E_\alpha = 13.5$ MeV. The shape of the curve is similar for the range of angles investigated. In both Figs. 9 and 10, the solid lines serve only to connect the points.

Because of space limitations we have included only a small number of the excitation curves and angular distributions measured for each reaction. These data and a discussion of the errors have been presented in a more complete form elsewhere[5] and are available to all who are interested. Additional data on $T(\alpha,n)Li^6$ and $He^4(He^3,p)Li^6$ may be obtained from the authors.

IV. THE PHASE-SHIFT ANALYSIS

A. Method

The first step in the analysis of the reduced data was the phase-shift analysis of both the Li^7 and Be^7 results. Both cases represent scattering of a spin-$\frac{1}{2}$ from a spin-0 particle. This fact greatly simplifies the analysis since only one l value is allowed for a given value of the total angular momentum and the parity. The formula for the differential elastic-scattering cross section is given as[6]

$$\frac{d\sigma(\theta)}{d\Omega} = |f_c|^2 + |f_i|^2, \tag{1}$$

where

$$f_c(\theta) = (-\eta/2k)\csc^2(\tfrac{1}{2}\theta)\exp[i\eta \ln \csc^2(\tfrac{1}{2}\theta)]$$

$$+\frac{1}{k}\sum_{l=1}^{\infty} e^{2i\alpha_l} P_l(\cos\theta)[(l+1)e^{i\delta_l^+}\sin\delta_l^+ + l e^{i\delta_l^-}\sin\delta_l^-],$$

and

$$f_i(\theta) = -\frac{1}{k}\sum_{l=0}^{\infty} e^{2i\alpha_l}\sin\theta \frac{dP_l(\cos\theta)}{d(\cos\theta)}$$

$$\times[e^{i\delta_l^-}\sin\delta_l^- - e^{i\delta_l^+}\sin\delta_l^+].$$

In these expressions:

θ is the center-of-mass scattering angle, k is the wave number, η is $Z_1Z_2e^2/\hbar v$, v is the relative velocity of the two particles, $\delta_l^{\pm} = \delta_{J\pi} = \delta_J^{\pi}$ is the phase shift for $j = l \pm \frac{1}{2}$, $\pi = (-1)^l$, $\alpha_l \equiv \omega_l - \omega_0$, where ω_l is the Coulomb phase shift, and Z_1 and Z_2 are the charges of the bombarding particle and the target nucleus.

The spin polarization of the scattered particles is given by $P(\theta) = [-2\,\mathrm{Im}(f_c f_i^*)]/[|f_c|^2 + |f_i|^2]$ in the direction of $(\mathbf{k}_{\rm in} \times \mathbf{k}_{\rm out})$, where $\mathbf{k}_{\rm in}$ and $\mathbf{k}_{\rm out}$ are unit vectors in the direction of the incident and scattered beams.

In both Be^7 and Li^7 the treatment of the reaction channels involving Li^6+a nucleon must be considered. This can be done by allowing the phase shifts to become complex, replacing $e^{2i\delta}$ by $\cos^2 X e^{2i\delta}$. Then $e^{i\delta}\sin\delta$ is replaced by $\cos^2 X e^{i\delta}\sin\delta + i[\frac{1}{2}(1-\cos^2 X)]$, and the total reaction cross section is given by

$$\sigma_R = (\pi/k^2)\sum_{l=0}^{\infty}[(2l+1)$$

$$-(l+1)(\cos^4 X_l^+) - l\cos^4 X_l^-]. \tag{2}$$

[5] R. J. Spiger, Ph.D. thesis, California Institute of Technology, 1967 (unpublished).

[6] C. L. Critchfield and D. C. Dodder, Phys. Rev. 76, 602 (1949).

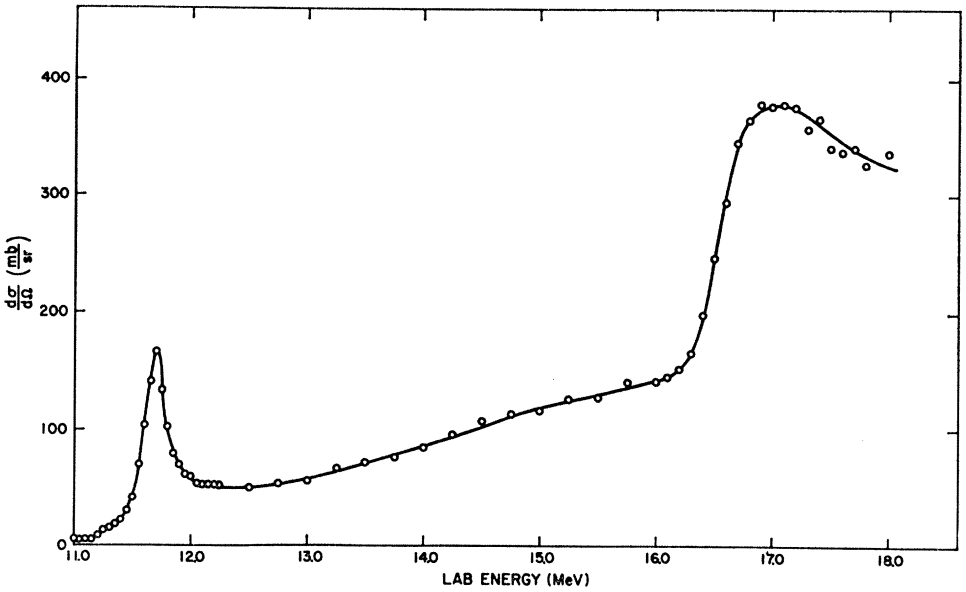

FIG. 6. Excitation curve for the $H^3(\alpha,n')$-Li^{6*} reaction showing the total reaction cross section for the $H^3(\alpha,n)$-Li^6 and $H^3(\alpha,n')Li^{6*}$ reactions. The data on $H^3(\alpha,n)Li^6$ below the $H^3(\alpha,n')Li^{6*}$ threshold provides normalization and background subtraction data thus allowing the effect of the $H^3(\alpha,n')Li^{6*}$ reaction to be separated. The line serves only to connect the points.

In the analysis, the real and imaginary part of the phase shifts from $l=0$ to $l=4$ could be varied. This gives a total of 18 parameters, although these were not all varied at one time. The data were grouped into angular distributions at the various energies of the excitation curves. A computer program was written to fit the data of each angular distribution with a set of phase shifts from Eq. (1) by minimizing the quantity

$$\chi^2=\frac{1}{N_\theta}\sum_{i=1}^{N_\theta}\left[\frac{(d\sigma/d\Omega)(\theta_i)_{\text{exp}}-(d\sigma/d\Omega)(\theta_i)_{\text{calc}}}{V(\theta_i)}\right]^2.$$

Here, N_θ is the number of data points in the angular distribution and $V(\theta_i)$ is the experimental error associated with each point.

B. The Analysis of the Be^7 Data

The phase-shift analysis of $He^4(He^3,He^3)He^4$ has been carried out from 2.5- to 5.7-MeV bombarding energy by Barnard[7] and from 5.75 to 12.0 MeV by Tombrello and Parker.[8] Because the splitting of the p waves of Tombrello and Parker differs in sign from those of Barnard, the analysis was performed over both these lower regions with the present data. The results could then be accurately extrapolated into the region above 12.0 MeV as trial phase shifts.

Below the first proton threshold at 7.0 MeV all values of $X_{J\pi}$ were held to zero and the real parts of the s, p, d, and f-wave phase shifts were allowed to vary. The initial values of the phase shifts were determined from Barnard's data. The general procedure was then to use the computer program to search for a set of phase shifts for which only one would be resonant at the anomaly in the elastic-scattering data. The selection of the $f_{7/2}$ phase shift was quickly accomplished, both by supplying trial phase shifts with a step in $\delta_{7/2}$ and by letting the program generate phase shifts at one energy using the phase shifts from the next lower energy for starting values. Several orders of phase-shift variation were tried with essentially the same result. The p- and s-wave phases were the most sensitive to the order of variation. Changing the order caused changes of $\pm 5°$ in the s and p waves. The phase shifts finally selected were those for which the variation with energy was smooth and the χ^2's were low.

Above 7-MeV bombarding energy, the reaction channel $He^4(He^3,p)Li^6$ is open. Data on the inverse reaction $Li^6(p,He^3)He^4$ were available and those of McCray[9] and Marion[10] were used to calculate the values of $X_{J\pi}$ from the total reaction cross section. The analysis of McCray attributes the cross section to a $\frac{5}{2}^-$ resonance and an s-wave background. We found that the background was too large to be accounted for by $X_{1/2}{}^+$. Therefore, $X_{1/2}{}^+$ was set equal to $X_{3/2}{}^+$ (d waves) and the sum of both terms was used for the nonresonant part of the reaction cross section, since both can correspond to emission of an s-wave proton. This choice gave slightly better fits than were obtained by using $X_{1/2}{}^+$ and $X_{3/2}{}^-$, but resulted in essentially the same phase shifts.

With the values of $X_{J\pi}$ fixed, the real phase shifts were then varied. The initial values were obtained by extrapolation from the lower region. The s, p, d, and f waves were varied and the appropriate resonant phase

[7] A. C. L. Barnard, C. M. Jones, and G. C. Phillips, Nucl. Phys. **50**, 629 (1964).
[8] T. A. Tombrello and P. D. Parker, Phys. Rev. **130**, 1112 (1963).
[9] J. A. McCray, Ph.D. thesis, California Institute of Technology, 1962 (unpublished).
[10] J. B. Marion, G. Weber, and F. S. Mozer, Phys. Rev. **104**, 1402 (1956).

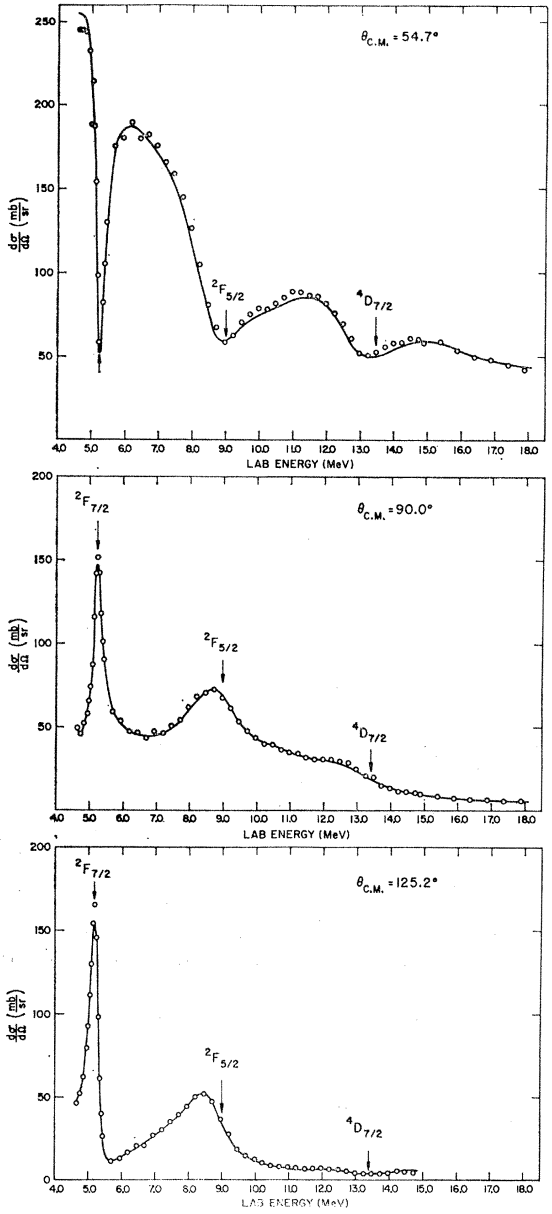

FIG. 7. Three typical excitation curves from the $He^4(He^3,He^3)He^4$ experiment. Symbols are the same as in Fig. 3.

shift proved to be $\delta_{5/2^-}$. As in the work of Tombrello and Parker,[8] the state at 7.18-MeV excitation energy was seen neither in the elastic-scattering data nor in the values found for the real part of the phase shift. Once again, several orders of variation of the phase shifts were tried. The f-wave phase shifts were stable to $\pm 2°$ and the s and p-wave phase shifts to $\pm 5°$ under the different variations. The solutions with good χ^2's also provided good energy continuity.

Above 11 MeV both the $He^4(He^3,p)Li^6$ and the $He^4(He^3,p')Li^{6*}$ channels are open. Our data on the first channel were used in conjunction with those of Marion[10] and McCray[9] to calculate values of $X_{5/2^-}$, $X_{3/2^+}$, and $X_{1/2^+}$ from 11 to 18 MeV. Data on the second reaction channel were limited to those obtained in the present work (Fig. 10). These data were used to form angular distributions at several energies near the resonance. Smooth curves were then drawn through the data points. Our data extended only to 120° in the center-of-mass system; hence it was necessary to extrapolate the data to 180° and to 0° to obtain total cross sections from these angular distributions. This was done by smoothly extending the curve to 0° and by assuming symmetry about 90°. The resulting curves were then numerically integrated to obtain the total cross section. These values (and the fact that the excitation curves for first-excited-state protons all had a similar shape) were then used to generate the total-reaction cross section as a function of the energy. An estimate was then made separating the curve into a resonant portion and a nonresonant background. The resulting resonance was too large to attribute to any single resonant $X_{J\pi}$ except $X_{7/2^-}$. The background was attributed to $X_{3/2^-}$ because of the proximity of the state at 9.8-MeV excitation energy seen by Harrison.[11] Using these values of $X_{J\pi}$, it was found that only a resonant $\delta_{7/2^-}$ phase shift would provide a fit low in χ^2 and continuous in energy. The features of the various phase shifts will be discussed in Sec. IV D.

C. The Analysis of the Li^7 Data

The target nucleus in these experiments was the lighter particle, thus requiring a higher bombarding energy to observe the same resonances. In the region of 3.6- to 11-MeV bombarding energy, there are no open reaction channels. Therefore, we set all the $X_{J\pi}=0$ in this region. As trial phase shifts, values from the Be^7 analysis taken below the first $\frac{7}{2}^-$ resonance were used. The s-, p-, d-, and f-wave phase shifts were then varied and the best values obtained at a given energy were used as trial values for the next energy. The program selected $\delta_{7/2^-}$ as the resonant phase shift for the lowest level. It also selected $\delta_{5/2^-}$ as the resonant phase shift for the broad second level. Several orders of variation of all the phase shifts were used to obtain smoothness in the phase shifts and low values of χ^2.

In the range from 10 to 11 MeV, some difficulty was encountered in obtaining good energy continuity in the $p_{1/2}$ and $f_{7/2}$ phase shifts. The $p_{3/2}$ and $f_{5/2}$ phase shifts were quite stable when different orders of variation were tried. These latter two phase shifts were finally fixed at their preferred values in this region and the other phase shifts were varied until a reasonably smooth set of phase shifts was obtained. Values of χ^2 were about 25% larger, in general, when the smooth set was used instead of a highly discontinuous set (e.g., variations of 30° in 250 keV for the $p_{1/2}$ phase shift).

The range of bombarding energies from 11 to 13 MeV was of particular interest. In analogy with the Be^7 data,

[11] W. D. Harrison, Ph.D. thesis, California Institute of Technology, 1966 (unpublished).

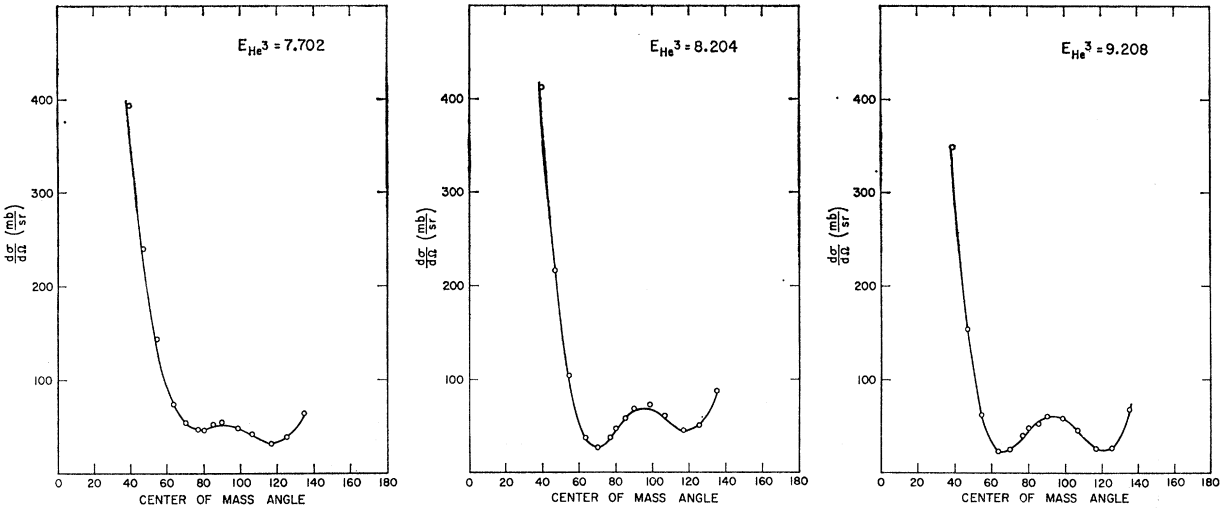

FIG. 8. Three typical angular distributions from the $He^4(He^3,He^3)He^4$ experiment. Symbols are the same as in Fig. 3.

the 7.47-MeV level (corresponding to the 7.18-MeV level in Be^7) was not expected to be seen in the elastic scattering. However, the effect of this level is apparent in the data as a small dispersion shape in the excitation curves.

The reaction channel $H^3(\alpha,n)Li^6$ is open in this region. The inverse reaction has been investigated by Schwarz[4] and his data were converted to our system and used to generate values of $X_{J\pi}$. His analysis indicated that the main effect was due to the $\frac{5}{2}^-$ resonance, with the nonresonant background being due to s-wave scattering of channel spin $\frac{1}{2}$. It was found that all of the background could be accounted for by the $X_{1/2}{}^+$ parameter alone; therefore, the $X_{3/2}{}^+$ parameter was not used. Using the values obtained for $X_{1/2}{}^+$ and $X_{5/2}{}^-$, and extrapolating the real phase shifts from lower energy, the program was used to see if $\delta_{5/2}{}^-$ would indicate a resonance behavior. No fit was obtained if a step-type behavior such as is seen in the two lower resonances was required. It was found that a dispersion shape curve in the $\frac{5}{2}^-$ phase shift gave the best fit. Attempts to fit the resonance with other phase shifts (such as $\delta_{7/2}{}^-$) did not succeed.

The presence of the resonance in Be^7 near 13.5 MeV indicated that an analogous effect might be observed in Li^7. Because the negative-ion injection beam was used, not as many data points were taken at each energy. All of the excitation curves indicated a more pronounced effect than was seen in Be^7, however.

Data on $H^3(\alpha,n')Li^{6*}$, other than our own, were not available. These data were decomposed into a smooth background and a resonance peak. From 13.5 to 18.7 MeV, the data of Murray and Schmitt[12] on the reaction $Li^6(n,\alpha)H^3$ were used to determine values of $X_{1/2}{}^+$ and $X_{3/2}{}^+$; the background in this region was too large to be accounted for by $X_{1/2}{}^+$ alone. The resonance peak which was separated from our $H^3(\alpha,n')Li^{6*}$ data was of such magnitude that it could only be accounted for by $X_{7/2}{}^-$.

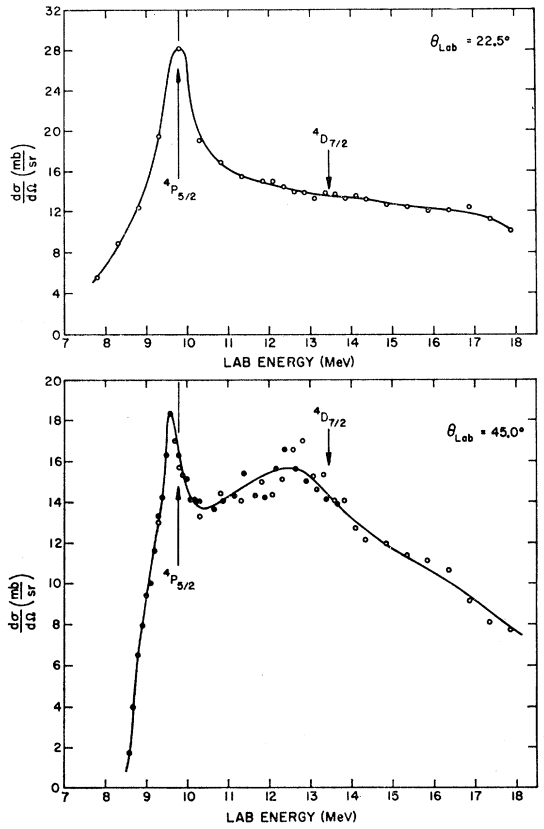

FIG. 9. Excitation curves for the $He^4(He^3,p)Li^6$ experiment showing the differential reaction cross sections for the $He^4(He^3,p)Li^6$ reaction at two typical laboratory angles. The open circles are the data obtained using the gas cell. The closed circles are data obtained by filling the whole chamber with target gas. The lines serve only to connect the points.

[12] R. B. Murray and H. W. Schmitt, Phys. Rev. **115**, 1707 (1959).

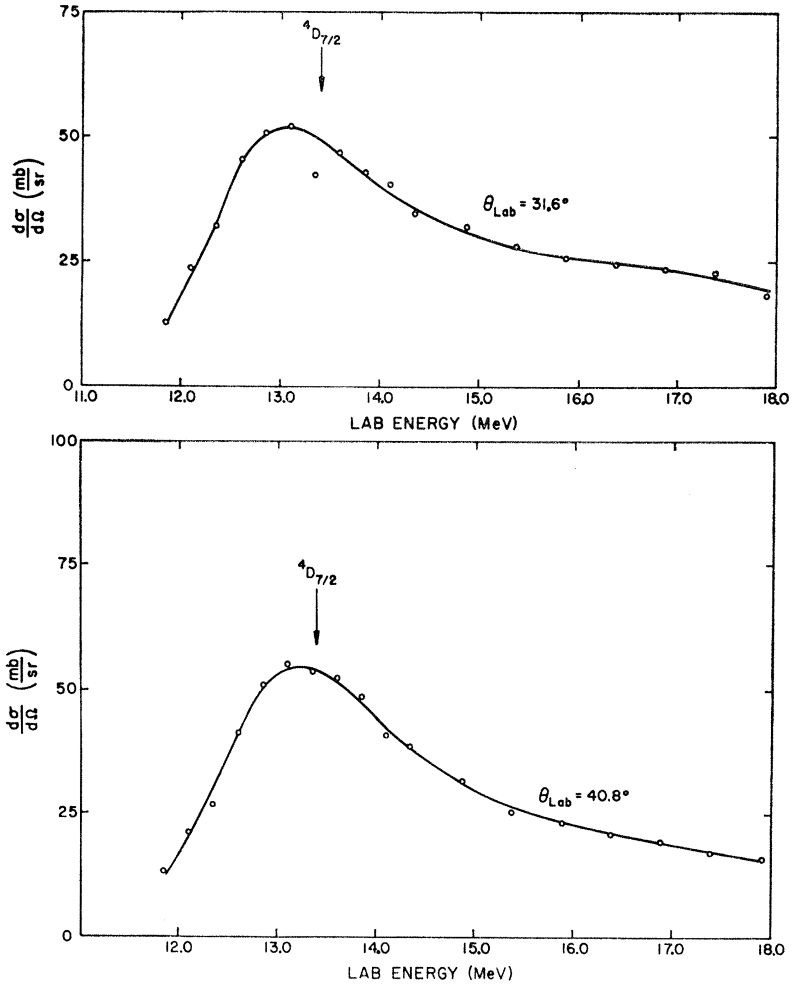

FIG. 10. Excitation curves for the $He^4(He^3,p')Li^{6*}$ reaction showing excitation curves of the first-excited-state protons for two laboratory angles investigated. The laboratory differential cross section is plotted versus beam energy. The lines serve to connect the points.

This was the same result as for Be^7. The nonresonant contribution to $H^3(\alpha,n')Li^{6*}$ was attributed to the $X_{3/2}^-$ term.

Using these values of $X_{J\pi}$, the real phase shifts were varied. Below the second-neutron threshold, the resulting phase shifts were continuous with the lower results. At 12.8- and 13.1-MeV bombarding energy, separate angular distributions were obtained using the beam from negative-ion injection and the beam from neutral-ion injection, respectively. Their separate analyses gave similar results, even though somewhat different values of the background $X_{J\pi}$ were used for each.

Above threshold, the resonant real phase shift was found to be $\delta_{7/2}^-$, as in the Be^7 case. However, it was not possible to obtain a good fit and maintain smooth behavior with energy of the supposedly nonresonant phase shifts. A variation of the $X_{J\pi}$ was tried, to accomplish this, but without success. The final values obtained for the phase shifts were a compromise between the best fit and the smoothest phase shifts, with good fit being the major consideration.

D. Discussion of the Phase Shifts and Polarizations

The phase shifts for $He^4(He^3,He^3)He^4$ are shown in Figs. 11–13. Phase shifts for $H^3(\alpha,\alpha)H^3$ are shown in Figs. 15–17. In both cases the various symbols represent values obtained from the phase-shift program and the lines show fits to these data using the R-matrix formalism. Tabulated values are available in Ref. 7.

S-Wave Phase Shifts

The s-wave phase shifts appear in Figs. 11 and 15. The dashed lines are calculated hard-sphere phase shifts for radii 2.8 F ($He^3+\alpha$) and 2.6 F ($t+\alpha$). There is a tendency in both cases for the phase shifts at higher energies to lie somewhat above the calculated curve. This effect has been noted previously in $He^4(He^3,He^3)He^4$ by Barnard[7] and by Tombrello and Parker.[8] McCray[9] suggested a $\frac{1}{2}^+$ level which might account for this behavior; such a level has not been seen in this work, however. The choices of $X_{J\pi}$ for the representation of the reaction cross section do have an effect and may account for the discrepancy.

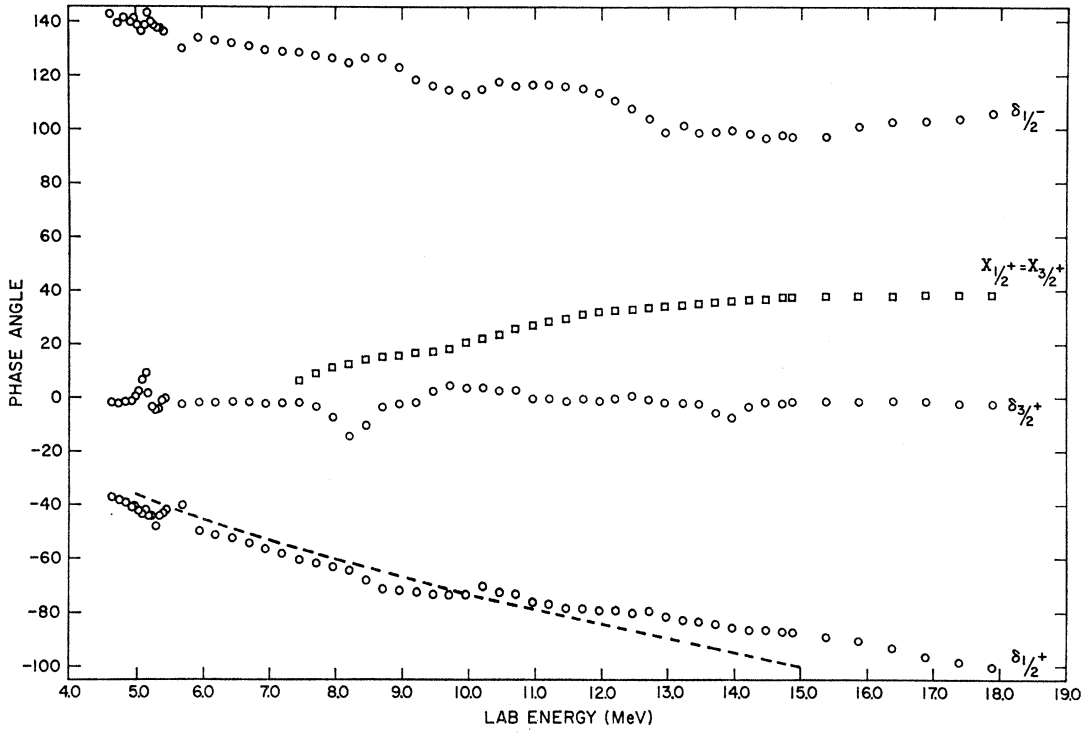

FIG. 11. $He^4(He^3,He^3)He^4$ phase shifts in degrees showing the phase shifts $\delta_{1/2}^+$, $\delta_{1/2}^-$, and $\delta_{3/2}^+$ as a function of energy. Also shown are the parameters $X_{1/2}^+$ and $X_{3/2}^+$. The dashed line is a fit to the phase shift $\delta_{1/2}^+$ and corresponds to the s-wave scattering from a hard sphere of radius 2.8 F.

P-Wave Phase Shifts

The $\frac{1}{2}^-$ phase shifts are shown in Figs. 11 and 15. The $\frac{3}{2}^-$ phase shifts appear in Figs. 12 and 16. With the exception of the f-wave phase shifts, these were the most difficult to determine. In the case of $He^4(He^3,He^3)He^4$, opposite splittings of the p-wave phase shifts were found by Barnard and by Tombrello and Parker. We therefore wished to investigate the sign of the splitting and to determine if there was a point at which the splitting reversed in sign. Both signs of the splitting were tried and that with $\delta_{3/2}^- > \delta_{1/2}^-$ was preferred in both $H^3(\alpha,\alpha)H^3$ and $He^4(He^3,He^3)He^4$. This result for Be^7 is in agreement with that of Barnard.

From the values in the figures, it is seen that these phase shifts have a very slight splitting at some energies. An example occurs near 11.5-MeV bombarding energy for $He^4(He^3,He^3)He^4$. Solutions with the opposite splitting were carefully investigated near these points and were found to be poorer than the solutions used.

Above 16-MeV bombarding energy in $H^3(\alpha,\alpha)H^3$, all the phase shifts, and the p-waves in particular are somewhat discontinuous with energy. This is an effect of the suggested $\frac{7}{2}^-$ level and probably reflects our lack of knowledge of the proper values of $X_{J\pi}$ used to represent the reaction cross section. The general fluctuations of the p waves elsewhere in both $H^3(\alpha,\alpha)H^3$ and $He^4(He^3,He^3)He^4$ are probably due in part to the fact that they and the f-waves are the only negative parity terms used in the analysis. Thus, the p-waves probably absorb a fair amount of any inaccuracies in the data which would tend to make the f-wave behavior less smooth.

D-Wave Phase Shifts

There are no d-wave levels in this energy range. The d-wave phase shifts were allowed to vary, but remained small over the total energy range in both cases. They are shown in Figs. 11 and 12 for $He^4(He^3,He^3)He^4$ and in Figs. 15 and 16 for $H^3(\alpha,\alpha)H^3$. Both the $\frac{5}{2}^+$ and $\frac{3}{2}^+$ phase shifts tend to remain near zero rather than decreasing at higher energy as for a hard-sphere phase shift. The points which depart from a smooth line for these phase shifts occur near resonances and the deviations are still relatively small. These excursions probably are the result of small inaccuracies in the data near the resonances.

F-Wave Phase Shifts

The f-wave phase shifts for $He^4(He^3,He^3)He^4$ appear in Fig. 13 while those for $H^3(\alpha,\alpha)H^3$ are shown in Fig. 17. The most obvious features are the sharp steps in the $\frac{7}{2}^-$ phase shifts. These show the second excited states in Be^7 and Li^7, thus indicating a $\frac{7}{2}^-$ assignment for this level in Li^7.

The broad step in the $\frac{5}{2}^-$ phase shifts indicates an assignment of $\frac{5}{2}^-$ for the level at 6.6 MeV in Li^7 and

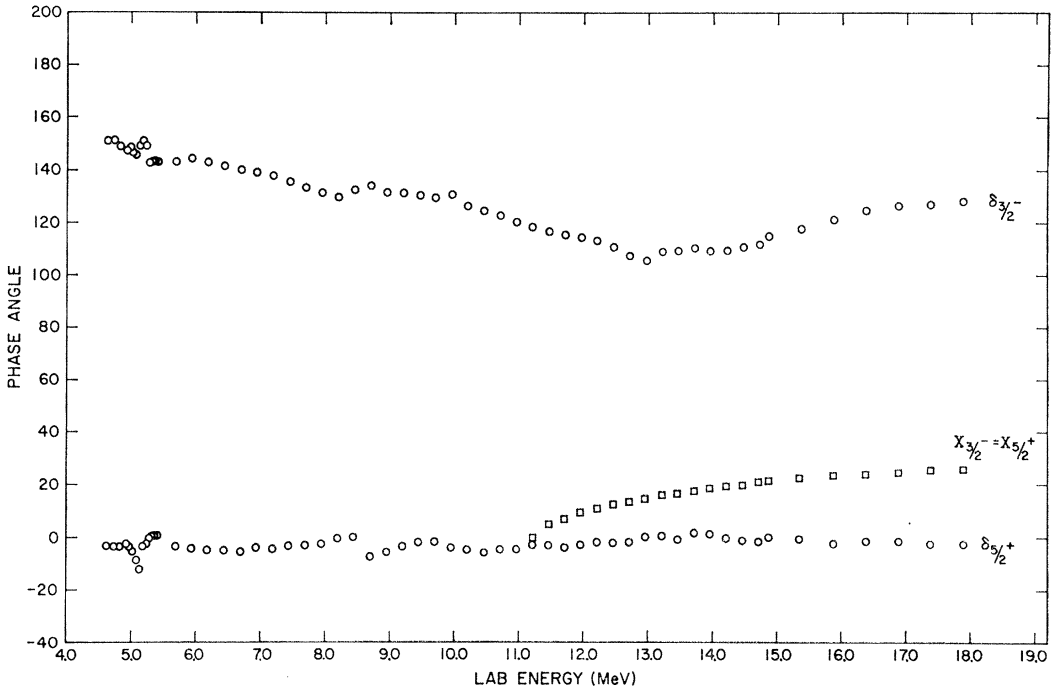

FIG. 12. $He^4(He^3,He^3)He^4$ phase shifts in degrees showing the phase shifts $\delta_{3/2^-}$ and $\delta_{5/2^+}$ as a function of energy. Also shown are the parameters $X_{3/2^-}$ and $X_{5/2^+}$.

confirms the $\frac{5}{2}^-$ assignment of Tombrello and Parker[8] for this level in Be^7.

The upper $\frac{5}{2}^-$ level was not seen in $\delta_{5/2^-}$ for $He^4(He^3,He^3)He^4$. It is seen in the parameter $X_{5/2^-}$, however. This result is not surprising since this level is also not seen in the elastic-scattering data. However, the corresponding Li^7 level does appear as a dispersion shape curve in $\delta_{5/2^-}$ at $E_\alpha=11.6$ MeV (Fig. 17) and as a peak in $X_{5/2^-}$ for $H^3(\alpha,\alpha)H^3$. A similar behavior is seen in the elastic scattering.

The dispersion curve shape appears in the $\frac{7}{2}^-$ phase shift for the level at 13.5-MeV bombarding energy in

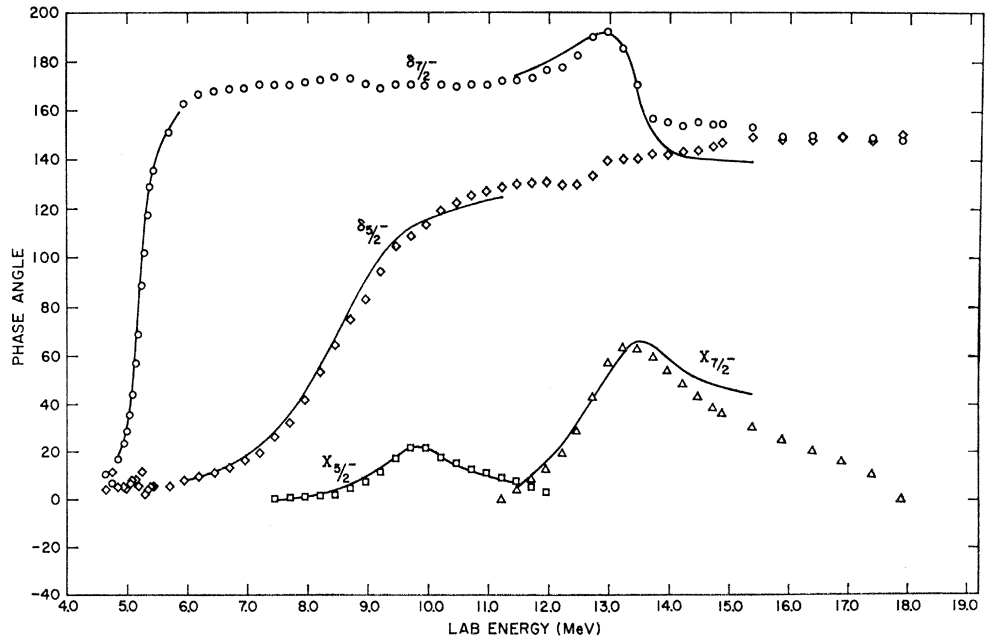

FIG. 13. $He^4(He^3,He^3)He^4$ phase shifts in degrees showing the phase shifts $\delta_{7/2^-}$ and $\delta_{5/2^-}$. Also shown are the parameters $X_{7/2^-}$ and $X_{5/2^-}$. The lines show the fits to the phase shifts from R-matrix theory.

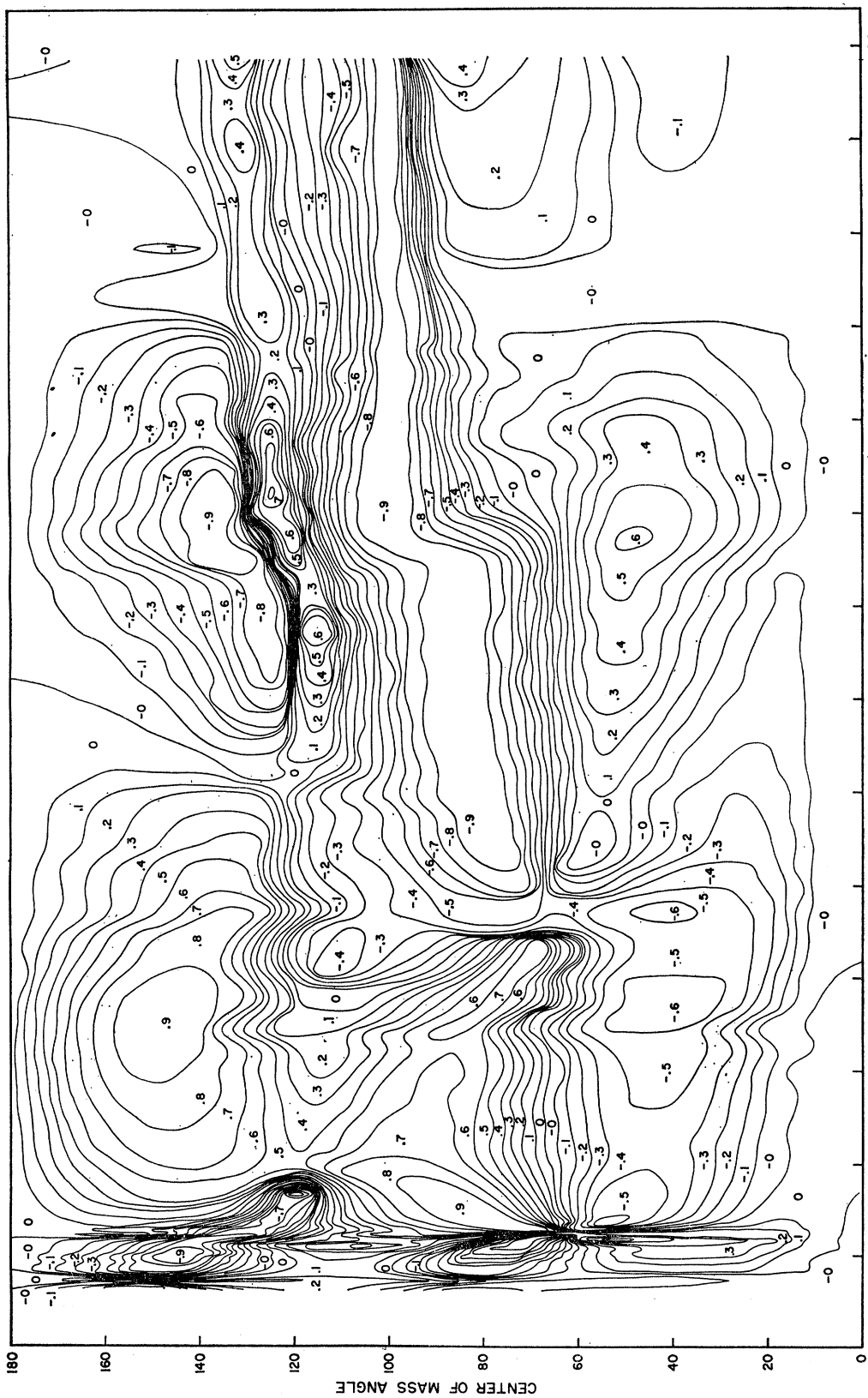

FIG. 14. The spin polarizations of the scattered He^3 particles from $He^4(He^3,He^3)He^4$. The polarizations are calculated from the phase shifts obtained in the phase-shift analysis. The Basel convention for the sign of the polarizations is used, and the contour levels are plotted as a function of center-of-mass angle and laboratory He^3 energy.

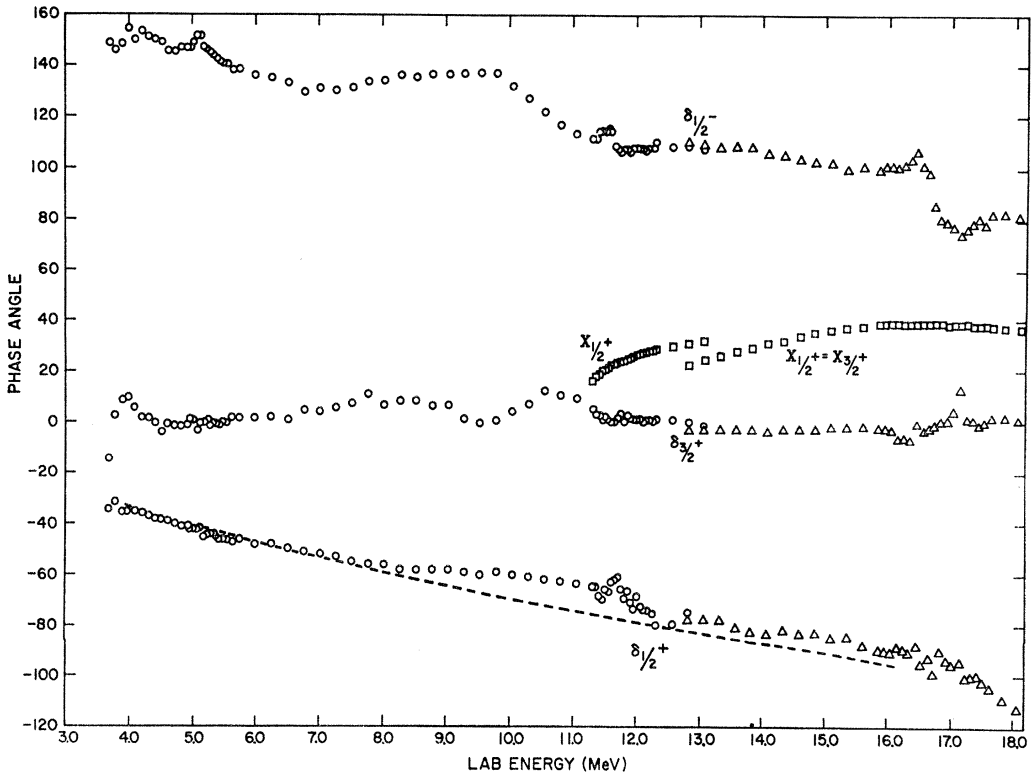

FIG. 15. $H^3(\alpha,\alpha)H^3$ phase shifts in degrees showing the phase shifts $\delta_{1/2}^+$, $\delta_{1/2}^-$, and $\delta_{3/2}^+$ as a function of energy. Also shown are the parameters $X_{1/2}^+$ and $X_{3/2}^+$. The dashed line is a fit to the phase shift $\delta_{1/2}^+$ and corresponds to the s-wave scattering from a hard sphere of radius 2.6 F. The change of symbols near 13 MeV indicates that the phase shifts and $X_{J\pi}$'s obtained above this energy used the negative ion injection-beam data. Below this energy, the neutral injection-beam data were used.

$He^4(He^3,He^3)He^4$ and for the level at 16.8-MeV bombarding energy for $H^3(\alpha,\alpha)H^3$. The level in Be^7 is much broader than that in Li^7. The $\frac{5}{2}^-$ phase shift is fairly smooth through the region of this resonance for Be^7; however, in Li^7, it varies by about 30° from a smooth curve. This effect persisted in the phase-shift analysis, despite efforts to eliminate it by adjusting other δ's or the $X_{J\pi}$'s. It was possible to reduce this variation by allowing the other nonresonant phase shifts to vary from a smooth curve to a greater extent. The variation of the nonresonant phase shifts is probably due to a combination of our poor reaction data and to a lack of knowledge about the possible effect of other levels in this region (e.g., the analog of the $\frac{3}{2}^-$ level seen by Harrison[11] in Be^7). In any case, the resonant behavior of the $\frac{7}{2}^-$ phase shift was independent of the behavior of the "nonresonant" phase shifts.

G-Wave Phase Shifts

No levels of $l=4$ have been found in either Be^7 or Li^7. These phase shifts were not varied during the analysis. At the conclusion of the analysis, they were allowed to vary and it was found that they remained small ($\leq\pm 2°$). Consequently, we felt justified in having neglected them in the analysis.

Polarizations

The polarizations for the He^3's and tritons were calculated from the derived phase shifts. The results are shown in Fig. 14 for $He^4(He^3,He^3)He^4$ and in Fig. 18 for $H^3(\alpha,\alpha)H^3$. Polarization contours are plotted versus center-of-mass angle and bombarding energy. The effects of the lower $\frac{7}{2}^-$ and $\frac{5}{2}^-$ levels are seen in both figures. As in the elastic scattering, the effect of the higher $\frac{5}{2}^-$ level is not seen in the He^3 polarizations while it is for the triton polarizations. The higher $\frac{7}{2}^-$ level is seen in both figures although it has a weaker effect for the He^3's than the tritons. This matches the relative effects in the elastic-scattering cross sections.

Of particular interest are the long regions of high negative polarization near 90°. These may be of use in polarization experiments as sources or analyzers of polarized particles.

V. EXTRACTION OF LEVEL PARAMETERS USING *R*-MATRIX THEORY

A. Method

The elastic scattering and reaction cross sections for two-particle interactions have been treated by Lane and Thomas.[13] This formalism connects the observed cross

[13] A. M. Lane and R. G. Thomas, Rev. Mod. Phys. **30**, 257 (1958).

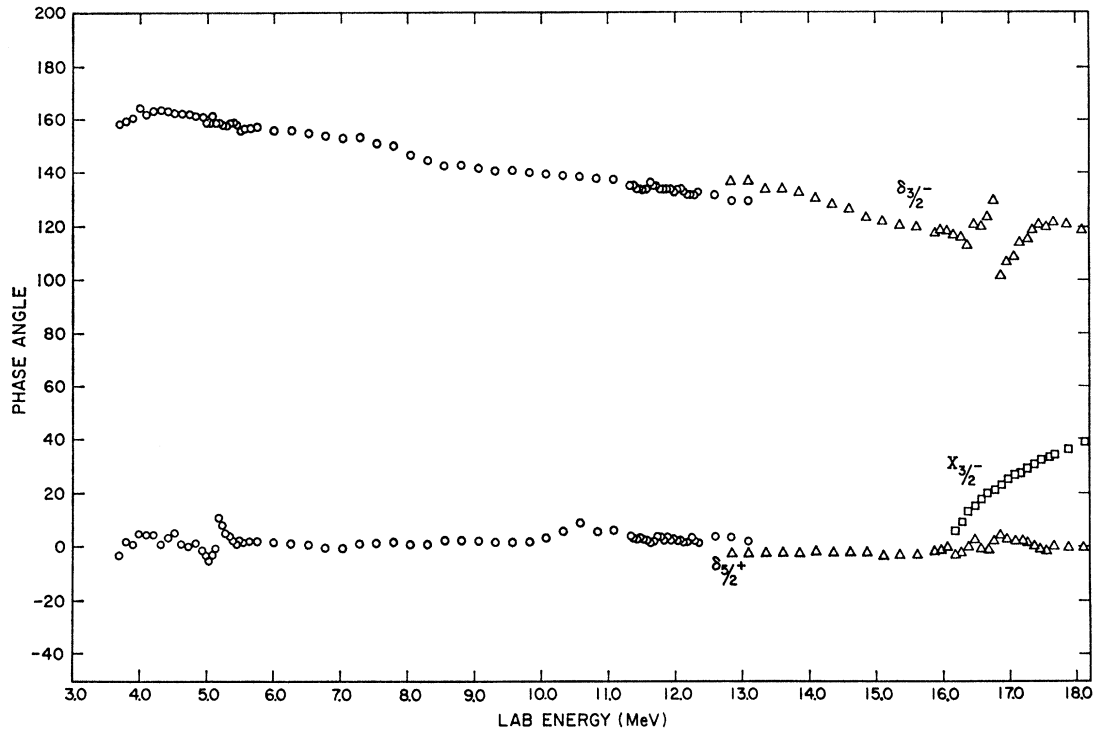

FIG. 16. $H^3(\alpha,\alpha)H^3$ phase shifts in degrees showing the phase shifts $\delta_{3/2}^-$ and $\delta_{5/2}^+$ as a function of energy. Also shown is the parameter $X_{3/2}^-$. The change of symbols near 13 MeV indicates that the phase shifts and $X_{J\pi}$'s obtained above this energy used the negative ion injection-beam data. Below this energy, the neutral injection-beam data were used.

section for a reaction or elastic scattering with a set of internal wave functions of the compound nucleus.

Our phase-shift analysis of the data provides the spins and parities of the states we have investigated in Li^7 and Be^7. This knowledge and the Lane and Thomas formalism are used to determine excitation energies and reduced widths for these states. For these reactions, the analysis is concerned with two levels (at most) of the same spin and parity. Also considered are an elastic channel and a reaction channel. Wave functions external to the nuclear surface are taken as the Coulomb wave functions or the analogous functions for the neutron channels. Following the notation of Lane and Thomas,[13] the appropriate R matrix is given as

$$R=\begin{pmatrix} R_{ee} & R_{er} \\ R_{re} & R_{rr} \end{pmatrix}=\begin{bmatrix} \dfrac{\gamma_{1e}^2}{E_1-E}+\dfrac{\gamma_{2e}^2}{E_2-E}, & \dfrac{\gamma_{1e}\gamma_{1r}}{E_1-E}+\dfrac{\gamma_{2e}\gamma_{2r}}{E_2-E} \\ \dfrac{\gamma_{1e}\gamma_{1r}}{E_1-E}+\dfrac{\gamma_{2e}\gamma_{2r}}{E_2-E}, & \dfrac{\gamma_{1r}^2}{E_1-E}+\dfrac{\gamma_{2r}^2}{E_2-E} \end{bmatrix}.$$

Here, r and e refer to the reaction and elastic channels. E_1 and E_2 are eigenenergies of the internal wave functions. E is the excitation energy of the nucleus. The γ's are the reduced-width amplitudes of the levels. (For example, γ_{1e}^2 is the elastic reduced width of level 1.)

The expression for the elastic channel collision matrix element is

$$U_{ee}=\Omega_{el}^2\left\{\frac{[1-R_{rr}(L_r-B_r)][1-R_{ee}(L_e^*-B_e)]-R_{re}^2(L_e^*-B_e)(L_r-B_r)}{[1-R_{rr}(L_r-B_r)][1-R_{ee}(L_e-B_e)]-R_{re}^2(L_e-B_e)(L_r-B_r)}\right\}=z/w.$$

The following definitions are employed:

$$L_c\equiv(\rho_c O_{cl}'/O_{cl})_{r_c=a_c}=S_{cl}+iP_{cl},$$

where S_{cl} is the shift function and P_{cl} is the penetration factor. $\Omega_{cl}=(I_{cl}/O_{cl})_{r_c=a_c}$. B_e and B_r are boundary values (taken as real in this work) for the elastic and reaction channels and are proportional to the logarithmic derivative of the internal wave functions at the nuclear radius a_c.

$\Omega_{el}^2=e^{2i(\omega_{el}-\varphi_{el})}$, where ω_{el} gives the Coulomb phase shift and φ_{el} gives the hard-sphere phase shift. In the phase-shift analysis, the Coulomb phase shift has been separated; therefore, one defines $\Omega_{el0}^2\equiv e^{-2i\varphi_{el}}$ and $U_{ee0}=(\Omega_{el0}^2/\Omega_{el}^2)U_{ee}=\cos^2 X_l e^{2i\delta_l}$, where δ_l and X_l are real. These definitions then give

$$\delta_l=-\varphi_{el}+\arctan[\mathrm{Im}(zw^*)/\mathrm{Re}(zw^*)],$$
$$X_l=\arccos(|U_{ee0}|^{1/2}).$$

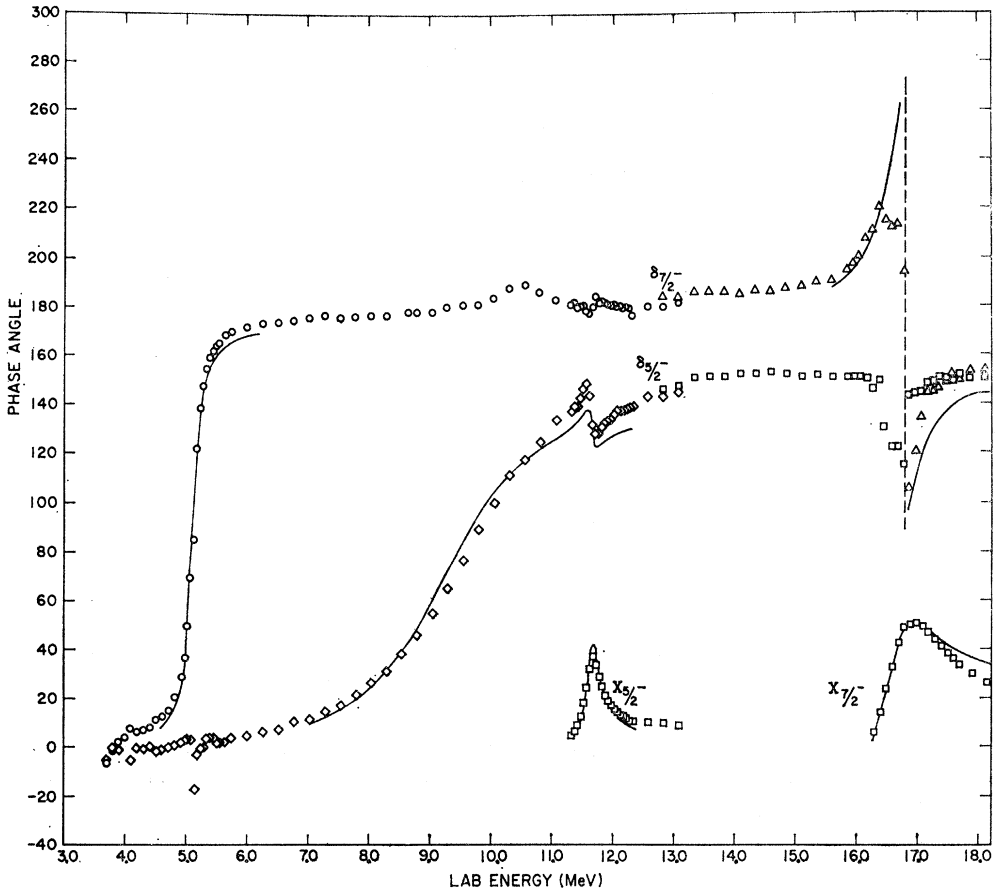

FIG. 17. $H^3(\alpha,\alpha)H^3$ phase shifts in degrees showing the phase shifts $\delta_{7/2^-}$ and $\delta_{5/2^-}$ as a function of energy. Also shown are the parameters $X_{7/2^-}$ and $X_{5/2^-}$. The change of symbols near 13 MeV indicates that the phase shifts and $X_{J\pi}$'s obtained above this energy used the negative ion injection-beam data. Below this energy, the neutral injection-beam data were used. The vertical dashed line near 17.0 MeV in the R matrix fit to $\delta_{7/2^-}$ indicates that either a step in the phase shift or a dispersion shape (as shown) is appropriate for this resonance. As the reaction width for the level increases, the R matrix fit changes smoothly from a step in $\delta_{7/2^-}$ to a dispersion shape. The best fit to the elastic scattering and reaction data gives the curve shown in the figure; this curve lies in the transition region between the two distinct forms.

We thus wish to compare δ_l and X_l with the $\delta_{J\pi}$ and $X_{J\pi}$ from the phase-shift analysis.

The relations are for a two-level problem with two open channels. If one takes the limiting case of one channel (elastic) and one level, then only R_{ee} remains. We then obtain

$$\delta_l = -\varphi_{el} + \arctan\left[\frac{\gamma_e^2 P_{el}}{E_\lambda + \Delta_\lambda - E}\right],$$

where

$$\Delta_\lambda = -\gamma_e^2 (S_{el} - B_e).$$

Comparison of the phase shifts to this single level formula can be approached as a linear least-squares fitting problem using γ_e^2 and E_λ as variable parameters. This will be done in the analysis for the second and third excited states of Li^7 and Be^7. The other levels are treated as double levels or as single levels with an open reaction channel.

B. Extraction of the Be^7 Level Parameters

The second excited state of Be^7 ($\frac{7}{2}^-$) is well below the threshold for $He^4(He^3,p)Li^6$. Because of this, the single-level formula (with only an elastic-scattering channel open) was used to fit the $\frac{7}{2}^-$ phase shift near this level. Several values of the radius were tried and 4.0 F was chosen as a suitable value. Good fits were also obtained for higher values of radius, but 4.0 F was more consistent with results for the other levels fitted in Be^7. For lower radii, the values of the eigenenergy and reduced width change very rapidly and fall outside reasonable limits. The values obtained are shown in Table I and the fits are shown in Fig. 13.

The two $\frac{5}{2}^-$ levels forming the third and fourth excited states in Be^7 have previously been analyzed as single levels because of the small reaction width of the $^2F_{5/2}$ level and the small elastic width of the $^4P_{5/2}$ level. In this analysis, the single-level formula was used to fit the lower level and obtain an elastic reduced width and eigenenergy. The reduced widths as given in Lauritsen and Ajzenberg-Selove[14] were then used for trial values for the higher state. The parameters obtained for the lower state from the single-level formula and the trial parameters for the upper state were then used in the double-level formula for both an elastic and a reaction channel. The trial parameters were found to give a good fit to the data. Variations of the eigenenergy or reduced width for the lower state produced poorer fits. Once again, 4.0 F was used as a radius for both states and both channels. Other radii were tried but the fits were

[14] T. Lauritsen and F. Ajzenberg-Selove, Nucl. Phys. **78**, 1 (1966).

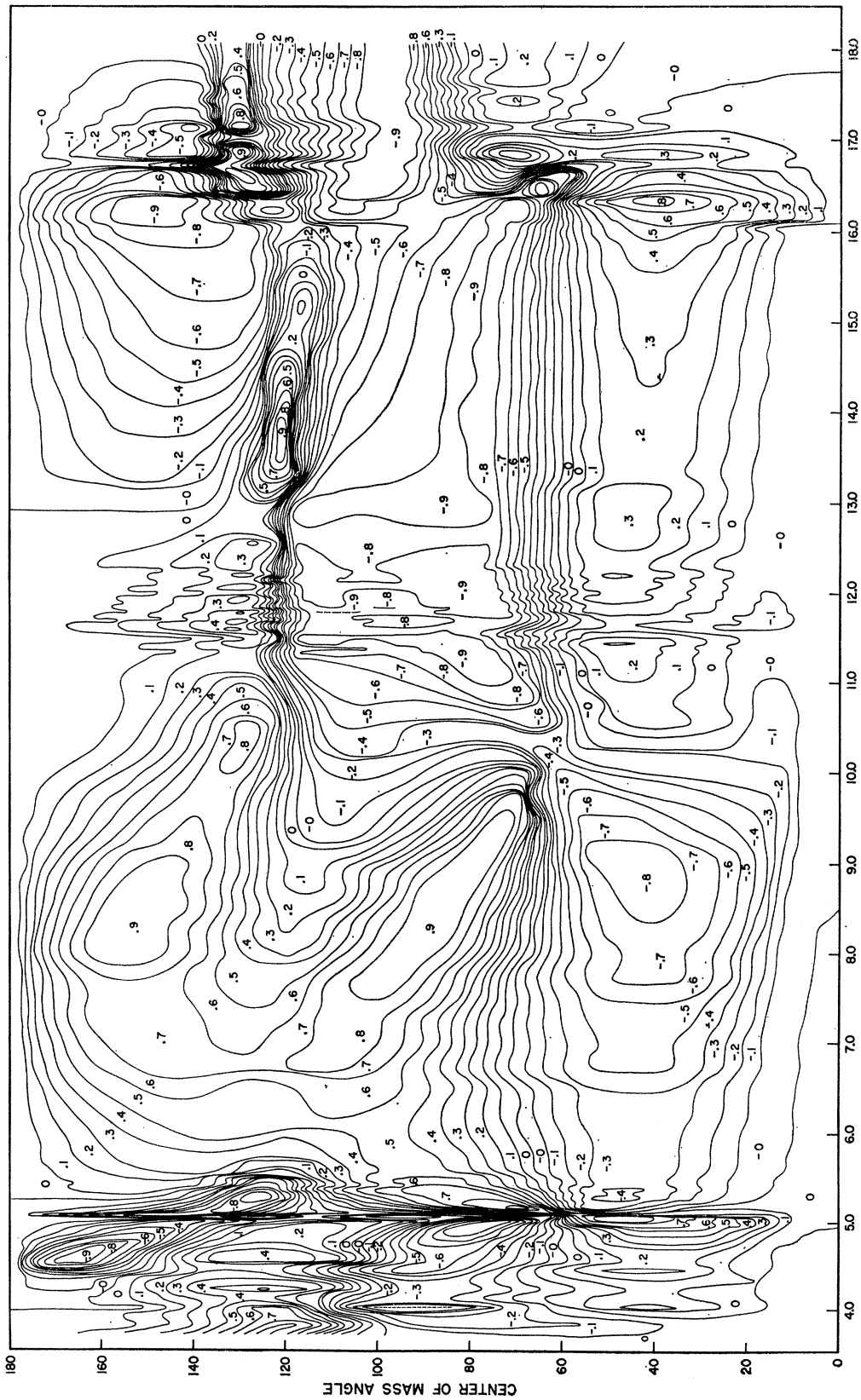

FIG. 18. The spin polarizations of the scattered tritons from $H^3(\alpha,\alpha)H^3$. The polarizations are calculated from the phase shifts obtained in the phase-shift analysis. The Basel convention for the sign of the polarizations is used and the contour levels are plotted as a function of center-of-mass angle and laboratory He^4 energy.

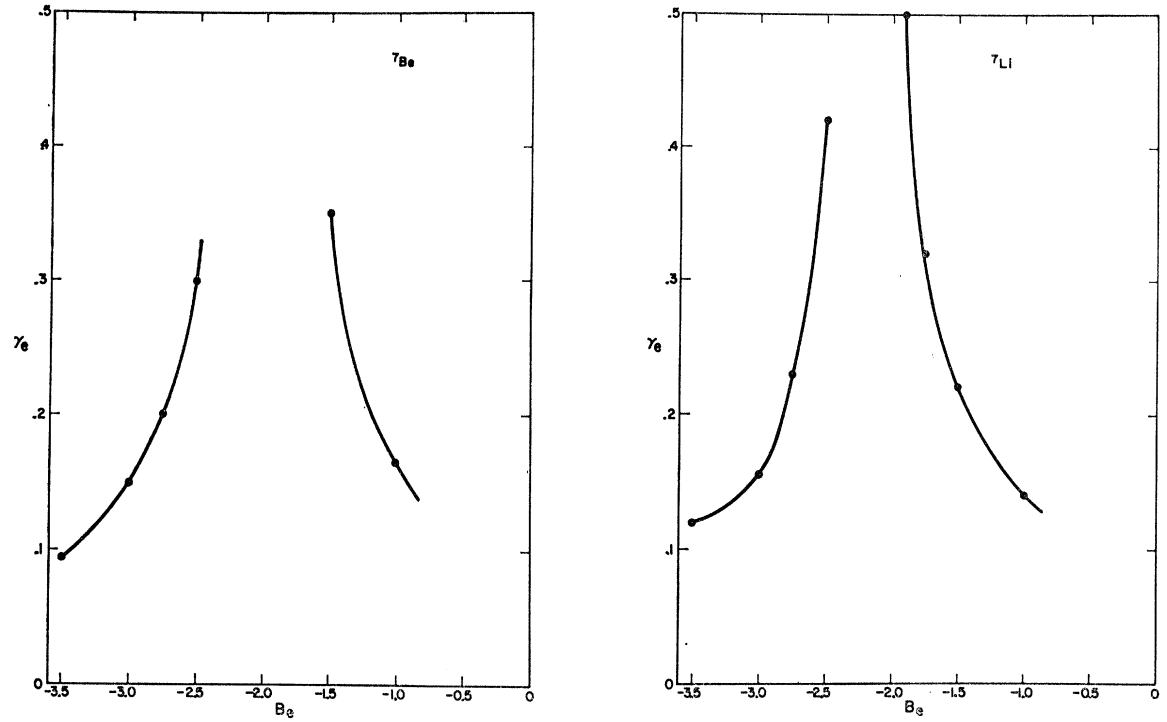

FIG. 19. Li^7 and Be^7 boundary value variations showing the value of the elastic reduced-width amplitude for the $^4P_{5/2}$ state in Li^7 and Be^7 which gives the best fit for a given value of the boundary value B_e. The lines are smooth curves connecting the calculated points.

not as good. With the eigenenergies and reduced widths fairly well determined, the reaction width for the lower level was varied from the starting value of zero. The values obtained for the various parameters are shown in Table I and the fits are shown in Fig. 13.

The boundary values used in the fitting (B_e and B_r) were set equal to $-l$ (the relative angular momentum of the two particles for each channel). This is a choice which is often used in the literature. Another common practice is to choose values which make the level shift zero at the resonance energy. For a single level, with or without a reaction channel, the two choices will give the same fit by simply adjusting the eigenenergy. For the double level formula, this is no longer the case. For the two $\frac{5}{2}^-$ levels in Be^7, it was found that the boundary value in the reaction channel still did not affect γ_e; however, to obtain a good fit when the elastic-channel boundary value was changed from $-l$, it was necessary to change the elastic reduced width of the upper level. For example, the use of the zero-level-shift boundary value required γ_e to be approximately 2.4 times as large as for the $-l$ case. The lower level was not appreciably affected. Some choices of boundary value and the corresponding best value of γ_e are shown in Fig. 19. The

TABLE I. Resonance energies and reduced widths. This table shows the resonance energies and reduced widths obtained for Li^7 and Be^7. A radius of 4.0 F was used for the analysis of all the levels. The subscripts n and p refer to the decay of the level to Li^6+nucleon. The subscripts n' and p' refer to the decay of the level to Li^{6*}+nucleon. $\theta_c^2 \equiv \gamma_c^2/(3\hbar^2/2\mu_c a^2)$ where a is the radius of interaction and μ is the reduced mass of the particle pair c. E_{res} is the excitation energy in the compound nucleus.

State	J^π	γ_α^2 (MeV)	θ_α^2	γ_n^2 (MeV)	θ_n^2	$\gamma_{n'}^2$ (MeV)	$\theta_{n'}^2$	E_{res} (MeV)
				Li^7				
$^2F_{7/2}$	$\frac{7}{2}^-$	1.3 ±0.1	0.57 ±0.04	...	...	...	...	4.65±0.05
$^2F_{5/2}$	$\frac{5}{2}^-$	3.1 ±0.3	1.36 ±0.13	0.00±0.01	0.000±0.002	...	...	6.64±0.10
$^4P_{5/2}$	$\frac{5}{2}^-$	0.024±0.003	0.011±0.001	1.2 ±0.1	0.26 ±0.02	...	...	7.47±0.03
$^4D_{7/2}$	$\frac{7}{2}^-$	1.2 ±0.5	0.53 ±0.22	...	...	10.6 ±3.0	2.3±0.7	9.67±0.10
				Be^7				
State	J^π	γ_α^2 (MeV)	θ_α^2	γ_p^2 (MeV)	θ_p^2	$\gamma_{p'}^2$ (MeV)	$\theta_{p'}^2$	E_{res} (MeV)
$^2F_{7/2}$	$\frac{7}{2}^-$	1.6 ±0.1	0.70 ±0.04	...	...	...	...	4.57±0.05
$^2F_{5/2}$	$\frac{5}{2}^-$	3.1 ±0.3	1.36 ±0.13	0.00±0.01	0.000±0.002	...	...	6.73±0.10
$^4P_{5/2}$	$\frac{5}{2}^-$	0.023±0.003	0.010±0.001	1.2 ±0.1	0.26 ±0.02	...	...	7.21±0.06
$^4D_{7/2}$	$\frac{7}{2}^-$	1.6 ±0.6	0.70 ±0.26	$1.3_{-0.8}^{+0.4}$	$0.29_{-0.18}^{+0.09}$	8.4 ±2.5	1.8±0.5	9.27±0.10

central region of B_e in this figure indicates no fit for γ_e up to 0.5. No fit appeared likely for values as high as 0.6 in this region.

The $\frac{7}{2}^-$ level at 9.3 MeV in Be^7 was first analyzed as a single level with a reaction channel and elastic channel open. A base line was determined from the $\frac{7}{2}^-$ phase shifts below resonance. This corresponded to 0° in the analyses. The reduced widths for elastic scattering and for the reaction leading to $Li^{6*}+p'$ were varied as was the eigenenergy of the state. A best fit was obtained for several radii and 4.0 F was again found to give the best results. Changing the boundary condition resulted only in a change in the best eigenenergy. The values obtained for the various parameters are shown in Table I and the fits are shown in Fig. 13.

As a final step, an attempt was made to fit the two $\frac{7}{2}^-$ levels with the double-level formula. To obtain a similar fit, it was necessary to reduce the reaction width of the top level and increase the elastic width. Unfortunately, the R-matrix phase shifts above the lower level drop off much like hard-sphere phase shifts. At the energy of the upper level, they were too low to give fits as good as the single-level fits obtained previously.

C. Extraction of the Li^7 Level Parameters

The extraction of the parameters for Li^7 was carried out in essentially the same manner as for Be^7. The second excited state $(\frac{7}{2}^-)$ is below the $H^3(\alpha,n)Li^6$ threshold and was treated as a single-channel single-level problem. Again, a best fit to the $\frac{7}{2}^-$ phase shift (for a given radius) was obtained. Here too, 4.0 F was chosen as a suitable radius. The values of excitation energy and reduced width for this level are shown in Table I and the fit to the $\frac{7}{2}^-$ phase shift is shown in Fig. 17.

The two $\frac{5}{2}^-$ levels forming the third and fourth excited states of Li^7 were analyzed as a double level. A single-level analysis of the broad lower level gave an eigenenergy and reduced elastic width. These values together with values of the reduced widths for the upper level[14] were used as trial values in the double-level formula. From these starting values, best values of eigenenergies and reduced widths were found. Changing the elastic reduced width and eigenenergy of the lower level produced poorer fits. The radius chosen was again 4.0 F. A variation of the reaction width of the lower level was also tried. The values obtained are shown in Table I and the fits to the $\frac{5}{2}^-$ phase shifts are shown in Fig. 17. The reduced α width is in good agreement with that obtained in the analysis of the $Li^6(n,\alpha)H^3$ data by Schwarz;[4] however, his nucleon width is $\sim 30\%$ higher than ours.

The boundary values used in the fitting were again taken as $-l$. A variation of the reaction channel boundary value changed only the eigenenergy, as in the Be^7 case. A change in the elastic-channel boundary value required both an eigenenergy change and a change in the value of the elastic reduced width for the upper level. Some cases are shown in Fig. 19. The behavior for central values of B_e is similar to that for Be^7.

As in the Be^7 case, the $\frac{7}{2}^-$ level near 9.7 MeV in Li^7 was fitted using a single level with both an elastic and a reaction channel. It was difficult to determine from the phase-shift analysis whether this level was best represented by a dispersion shape or step shape in the phase-shift curve. Slightly better results were obtained with a dispersion shape in the phase-shift analysis, but the R-matrix formalism gave a better fit using a step shape. Once again 4.0 F was obtained as the best radius. The fit is shown in Fig. 17 and the values of the reduced widths are shown in Table I. The vertical dashed line shows the point in energy above which 180° has been subtracted from the calculated phase shifts to compare them with the values obtained in the phase-shift analysis.

D. Discussion of the Derived Level Parameters

The fitting of the s-wave phase shifts by hard-sphere scattering phase shifts has been discussed in Sec. IV D.

An attempt was made to determine the reduced widths of the ground state and first excited state in Li^7 and Be^7 by fitting the p-wave phase shifts. Reasonable fits were obtained at most radii used, but the values of the resonance parameters were not reasonable. Many of the reduced widths were negative and none predicted the proper locations for the levels.

There are no known d-wave levels in the two nuclei and the d-wave phase shifts remain small and inactive in the analysis. Therefore, no attempt was made to fit these phase shifts with the R-matrix formalism.

Good fits to the second excited state $(\frac{7}{2}^-)$ of both Be^7 and Li^7 were obtained with the single-level, single-channel R-matrix formalism. The reduced widths agree quite well between the nuclei. In addition, the use of the same radius as that used by Barnard[7] (4.4 F) yields a reduced width in agreement with his results to within the expected errors. The reduced widths for the states tend to increase fairly rapidly as the radius is decreased from 4.4 F.

The elastic reduced widths of the lower $\frac{5}{2}^-$ level in both nuclei were also obtained using the single-channel, single-level formalism. Good fits were obtained except for the regions on the upper edge of the lower $\frac{5}{2}^-$ levels. Here the phase shifts calculated from the R-matrix formalism lie below those obtained from the phase-shift analysis. This difficulty was not (as was previously hoped) resolved by analyzing the two $\frac{5}{2}^-$ levels in each nucleus with the two-channel, two-level R-matrix formalism. The nucleon reduced widths of the lower $\frac{5}{2}^-$ levels were determined from the double-level formula and were quite small in both cases. The errors for these reduced width amplitudes are quite large, but the fits to the phase shifts indicate that they have a negative sign in both Li^7 and Be^7. The agreement of the reduced

widths of the lower $\frac{5}{2}^-$ levels between the nuclei is very good. However, for Be^7 the reduced width obtained for this level is considerably larger than the value obtained by Tombrello and Parker,[8] even when the difference in radii is considered. This difference may be a result of the difference of sign in the splitting of the p-wave phase shifts in the two analyses.

The analysis of the $^4P_{5/2}$ levels was done with the double-channel, double-level formula in both nuclei. Good fits were obtained for Be^7 using values in agreement with those reported.[14] The fits obtained for Li^7 were a compromise between a good fit to the elastic phase shift $\delta_{5/2^-}$ and a good fit to the $X_{5/2^-}$ parameter. The values obtained are in agreement with those given in Ref. 14. There is also good agreement between the two nuclei.

The level at 9.3 MeV in Be^7 ($\frac{7}{2}^-$) was analyzed as a two-channel, single-level problem. The fits are least accurate on the high side of the resonance. This may well be a result of the errors in the reaction data used to fix the values of $X_{7/2^-}$ for this level. The reduced width for $Li^{6*}+p'$ is seen to be much larger than that for $He^3+\alpha$. The decay of this level appears to proceed almost entirely by $Li^{6*}+p'$. Recent work by Christensen and Cocke[15] has shown the presence of a small f-wave admixture in the configuration of the 2.43-MeV state in Be^9. The decay of the 9.3-MeV level in Be^7 also offers an opportunity to determine such an f-wave admixture. The predominant mode is $Be^7(9.3) \rightarrow Li^6(2.184, 3+)+p$ by a p-wave decay. The decay of this level to Li^6(g.s.)$+p$ requires the Li^6 and p to be in a relative f-state of angular momentum. Thus, the ratio of the reduced widths for these two channels is a measure of the relative f-wave admixture in the level. A small amount of yield in the ground-state protons was attributable to the decay of the 9.3-MeV level. The effect was seen at several angles. These data were used to form angular distributions from which the total cross section was crudely determined. The ratio of $\gamma^2_{\text{g.s.}}/\gamma^2_{\text{1st ex.}}=\gamma^2_{f\text{ wave}}/\gamma^2_{p\text{ wave}}$ was determined by the relation $(\sigma_{\text{g.s.}}P_1)/(\sigma_{\text{1st ex.}}P_3)\approx\gamma^2_{\text{g.s.}}/\gamma^2_{\text{1st ex.}}$ which applies at the resonance energy. P_l gives the penetration factor for each decay. The value obtained for the ratio of reduced widths was $(16_{-10}{}^{+5})\%$. The high errors reflect the small size of the effect and the uncertainty in separating it from the large nonresonant background. This figure represents a value of $(1.3_{-0.8}{}^{+0.4})$ MeV for the reduced width for ground-state protons.

The upper $\frac{7}{2}^-$ level in Li^7 was treated in the same manner as the corresponding level in Be^7. Although the results of the phase-shift analysis were not as satisfactory, the values of reduced widths agree fairly well between the two levels. From our data, it was not possible to obtain an estimate of the f-wave admixture in this level. The effect of this admixture does not appear in the excitation curves taken at several angles for the $H^3(\alpha,n)Li^6$ reaction. However, the scatter of the data points, due to background subtraction, could conceal a somewhat smaller effect than that seen in Be^7.

The fits to the phase shifts were found to be consistently best for a radius of 4.0 F. For the first $\frac{7}{2}^-$ level and first $\frac{5}{2}^-$ level in both nuclei, a larger radius gave a similar fit and required a smaller reduced width. For the $^4P_{5/2}$ levels, a larger radius (4.4 F) produced a poorer fit. The best results for the higher $\frac{7}{2}^-$ levels also required a radius of 4.0 F.

The behavior of the reduced widths as a function of boundary value was of considerable interest. Figure 19 shows the value of the elastic reduced-width amplitude (γ_e) as a function of the elastic boundary value B_e. The value of γ_e is that which best fits the phase shifts for that value of B_e. The regions of B_e near -1.6 are where the boundary value results in zero-level shift. Note the region of very high γ_e between this region and $B_e=-3.0$ or $-l$. The effect is similar in both nuclei and only occurs where the double-channel double-level formula is used. For a radius of 4.0 F, changing the value of the inelastic boundary value had the effect of changing only the eigenenergies. At other radii (such as 4.4 F), the inelastic boundary value also had a similar effect on the best value of γ_e. We used $B_e=-l$ in extracting the reduced widths given in Table I.

VI. MODEL COMPARISONS

A. The Cluster Model

Several calculations have been made in an attempt to treat Li^7 and Be^7 as two clusters of nucleons such as an α particle and a triton.[16] A variational procedure is used with trial wave functions to determine an upper bound to the energies of various levels. The wave functions consist of an internal wave function for each cluster and a wave function describing the relative motions of the clusters. The potential used is a finite depth central potential taken between each pair of particles. In Ref. 16 a spin-orbit potential is also considered. The calculations were done for the ^2P and ^2F levels in Be^7 and Li^7, which should be well represented by the α+mass-3 cluster scheme. The calculated energy levels agree fairly well with the first and second excited states. The $^2F_{5/2}$ level is predicted at a lower energy than is found experimentally. In a later paper,[17] a Li^6+n cluster calculation is made and an approximate number is obtained for the position of the $^4P_{5/2}$ level. At the same time, it is shown that a positive parity level near 6.5 MeV in Li^7 is unlikely.

The cluster-model calculations are of interest for several reasons. They show that the grouping of the

[15] P. R. Christensen and C. L. Cocke, Nucl. Phys. **89**, 656 (1966).

[16] Y. C. Tang, K. Wildermuth, and L. D. Pearlstein, Phys. Rev. **123**, 548 (1961).

[17] F. C. Khanna, Y. C. Tang, and K. Wildermuth, Phys. Rev. **124**, 515 (1961).

nucleons into these clusters can be a reasonable approach to the problem. The number of parameters which are varied to obtain the energy levels is smaller than in the usual shell model calculations. Also, an attempt is made to use two-body central forces (derived from nucleon-nucleon scattering) between individual particles instead of placing the p-shell nucleons in a common potential well.

There are also some disadvantages. The calculations are mainly limited to the lowest levels of Li^7 and Be^7, where only a single two-body configuration is important. Because the trial wave functions are suitable for bound states and hence do not provide information on the particle scattering, the calculated positions of the higher energy levels tend to disagree with the experimental values.

B. The Rotational Model

Consideration has also been given to the rotational model as a description for the light nuclei. In particular, Chesterfield and Spicer[18] have made calculations for Li^7 (and Be^7) using this model. The model calculates the energy for a number of configurations using a Nilsson model potential. These energies are calculated as functions of a deformation parameter ϵ which is a measure of the nonsphericity of the harmonic oscillator well used in the potential. The energy minimum for each configuration is used to determine the best value of ϵ.

Each configuration is then used as a basis state for the formation of a rotational band. If the energy of a basis configuration is given by $E_K{}^0$ then the energies of the other levels of the band are given by

$$E(I)=E_K{}^0+A[I(I+1)+\delta_{K,1/2}a(-1)^{I+\frac{1}{2}}(I+\tfrac{1}{2})],$$

where $A=\hbar^2/2I_i$ (I_i is the nuclear moment of inertia), I is the total angular momentum of the nucleus, and "a" is a decoupling parameter defined by Nilsson.[19] K is the projection of I on the body z axis. A is chosen to give a best fit to the data. Of the six bands considered in these calculations, three are of positive parity. Since no positive parity levels were found in this experiment, we will not consider them further. The band based on the $\frac{1}{2}^-$ level at 0.48 MeV seems to represent the ground state and first three excited states quite well. The second band based on a $\frac{3}{2}^-$ level at 5.62 MeV predicts the $^4P_{5/2}$ level and has a $\frac{7}{2}^-$ level near an energy appropriate to the position of the new $\frac{7}{2}^-$ level found here. The $\frac{3}{2}^-$ state forming the basis for this band does not appear to exist and is evidently a spurious representation of the ground state. The third band is based on a $\frac{1}{2}^-$ level which also has not been observed. A $\frac{3}{2}^-$ level in this band could represent the level seen by Harrison[11] at 9.8 MeV in Be^7. The other members of this band have not been identified. The calculated levels which fit our current level scheme are shown in Fig. 20(b).

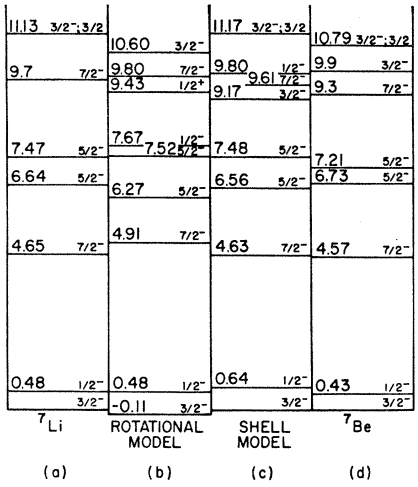

FIG. 20. Nuclear model predictions of the energy levels for Li^7 or Be^7 with their spins, parities, and isospins as predicted by the rotational model (Ref. 18) (b) and the shell model (Ref. 1) (c). Parts (a) and (d) show Li^7 and Be^7 energy levels determined by experiment. The isospin is $\frac{1}{2}$ except for those levels listed as $T=\frac{3}{2}$.

This model reproduces the lowest five levels in Li^7 and Be^7 quite well (with the exception of the $\frac{3}{2}^-$ basis of the second band). It also gives good agreement with experiment for the ground-state electromagnetic moments, the de-excitation of the first excited state and the decay of Be^7. The use of this model to calculate the f-wave nucleon decay of the new $\frac{7}{2}^-$ level gives values of $\gamma^2{}_{f\text{ wave}}/\gamma^2{}_{p\text{ wave}}$ from 0.06 to 0.22 for values of ϵ from 0.4 to 0.8. The energy minimum for the band occurs at $\epsilon=0.4$.

The model has, of course, the problem of trying to represent a continuum situation with bound-state wave functions. Thus the scattering of particles has not been considered, nor have reduced widths for various configurations for the levels been calculated. The basis states of the second and third bands are also a problem since they do not appear to exist; however, it appears that these levels can be eliminated from the predictions without changing the remainder of the calculation.

C. The Shell Model

Most of the calculations for Li^7 and Be^7 have made use of the shell model. The model normally considers negative (normal) parity levels formed by a $(1s)^4(1p)^3$ configuration. Several surveys of the light nuclei (including Be^7 and Li^7) have been made using the shell model.[20,21] The energy levels obtained by Barker[1] are in agreement with the schemes found in these earlier calculations. These energy level schemes for Be^7 and Li^7 are shown in Fig. 20(c). Also shown in Fig. 20 are the rotational-model predictions and the experimental re-

[18] C. M. Chesterfield and B. M. Spicer, Nucl. Phys. **41**, 675 (1962).

[19] S. G. Nilsson, Kgl. Danske Videnskab. Selskab, Mat.-Fys. Medd. **29**, No. 16 (1955).

[20] D. R. Inglis, Rev. Mod. Phys. **25**, 390 (1953).

[21] D. Kurath, Phys. Rev. **101**, 216 (1956).

sults. The first four excited states of Li^7 and Be^7 show agreement in energy and configuration with experimental observations. We have identified our highest level with his $\frac{7}{2}^-$ level which consists mainly of the $^4D_{7/2}$ configuration. Our relative nucleon and α widths for this level are in good qualitative agreement with the predicted configuration. The energy predicted for the $^4D_{7/2}$ level also fits our experimental data. The calculation predicts a $\frac{3}{2}^-$ level below the $\frac{7}{2}^-$ level, whereas the data on Be^7 from our work and that of Harrison show the $\frac{3}{2}^-$ level at a higher energy than the $\frac{7}{2}^-$ level.

The model calculations predict assignments of $\frac{1}{2}^-$, $T=\frac{1}{2}$ and $\frac{3}{2}^-$, $T=\frac{3}{2}$ for the 7th and 8th excited states. The $\frac{1}{2}^-$, $T=\frac{1}{2}$ level has not been seen, but the $\frac{3}{2}^-$, $T=\frac{3}{2}$ level of Harrison's work,[11] or that of Cerny, *et al.*,[22] is in agreement with the predictions.

The predictions of this nuclear model appear to be quite good even though the problem is not considered in the continuum. Since the only configuration considered is $(1s)^4(1p)^3$, the problem of the positive parity levels does not arise. The ground-state magnetic moment, $\log ft$ values for the Be^7 decay and the lifetime of the first excited state are also calculated and agree with the experimental values. Quantities such as the quadrupole moments depend sensitively on configuration mixing and since this was not considered, the calculated values do not give a good fit to the experimental values.

The models discussed all make fairly good predictions for the lower levels. It is to be expected that the more recent shell-model calculations of Barker will give better agreement for the higher energy levels. This agreement results from a greater abundance of experimental data and also from a larger number of fitting parameters than were used in the rotational model. None of the models, however, has attempted to describe the various particle-scattering processes.

VII. CONCLUSIONS

The previous section has shown the qualitative agreement between the predictions of nuclear models and the results of this work. It is also worthwhile to point out the agreement between the experimental results for the two nuclei. This is especially evident in the reduced widths for the various levels. The two $\frac{5}{2}^-$ levels show excellent agreement between the two nuclei and the agreement for the two $\frac{7}{2}^-$ levels is also quite good.

The agreement of the nonresonant phase shifts between the two nuclei is also good. The p-wave phase shifts in particular show the same sign for the splitting and the same energy behavior in both nuclei. In our work, however, we were unable to account for the behavior of the p waves in terms of the influence of the ground and first excited states in Li^7 and Be^7. Whether this behavior can be explained by high-energy p-wave levels remains open to question.

The existence of positive parity states in the range of this work has been a question for some time. For example, a paper by Lane[23] uses configurations $(1s)^4(1p)^2 2s$, $(1s)^4(1p)^2 1d$, and $(1s)^3(1p)^4$ to predict many low-lying, positive-parity levels. Earlier experiments on Be^7 as well as this work have found no evidence for a positive parity level within the energy range investigated.

In the R-matrix analysis, the calculated phase shifts have a general tendency to lie below those obtained from the data on the high-energy side of a resonance. It does not appear that one can account for this by errors in the phase-shift analysis since the effect has the same sign for all the resonances.

The behavior of the reduced widths as a function of the boundary value in the R-matrix analysis is also a matter of some concern (see Fig. 19). These results indicate that in the double-level analysis, it is possible to fit the data with a range of γ_c's which vary by a factor greater than 5. Although this problem did not occur for the single-level analyses, it is still rather disturbing and should be investigated further.

The work which has been described examines a large energy range for both Li^7 and Be^7. While good agreement between the two nuclei and with the nuclear shell model has been shown, there are still several problems of interest.

ACKNOWLEDGMENTS

The authors wish to thank A. D. Bacher and H. T. Larson for their assistance in the preparation and execution of the experiments. The assistance of D. Papanastassiou, R. Moore, and G. Fox in reducing the data is also greatly appreciated.

[22] J. Cerny, C. Détraz, and R. H. Pehl, Phys. Rev. **152**, 950 (1966).

[23] A. M. Lane, Rev. Mod. Phys. **32**, 519 (1960).